THE ASTRONOMICAL JOURNAL VOLUME 106, NUMBER 3 SEPTEMBER 1993

ON THE NATURE OF Mg II ABSORPTION LINE SYSTEMS IN QUASARS

M. J. DRINKWATER
Anglo-Australian Observatory, Coonabarabran, NSW 2357, Australia, and Observatoire du Mont Mégantic, Université Laval, Québec, Canada
Electronic mail: mjd@aaocbn.aao.gov.au

R. L. WEBSTER
School of Physics, University of Melbourne, Parkville, Vic. 3052, Australia
Electronic mail: webster@tauon.ph.unimelb.edu.au

P. A. THOMAS
MAPS, University of Sussex, Brighton BN1 9QH, United Kingdom
Electronic mail: petert@syma.sussex.ac.uk

Received 1993 January 8; revised 1993 May 10

ABSTRACT

The results of a large R-band imaging survey of 71 bright ($m_V < 18$) quasars are presented. The quasars were chosen from published samples which have intermediate resolution optical spectroscopy available, so the presence of low redshift Mg II absorption lines can be determined. We have searched our data for galaxies close to the line-of-sight to the quasars, which we might be able to identify with the absorption systems. We find a high coincidence between galaxies very near the line-of-sight and quasars showing absorption systems in their spectra, a result consistent with other studies. These galaxies have a mean luminosity of $0.5L_*$ (assuming they lie at the absorption redshift). The distribution of impact parameters between the galaxies and the quasars extends with a flat distribution to large radii ($> 30h^{-1}$ kpc). This suggests that the absorption systems may not be gravitationally bound to the observed galaxies, but may be part of larger extended systems. We also find a significant number of galaxies near the line-of-sight to the quasar where no absorption is seen in the quasar spectrum. The selection of our quasars is unbiased with respect to galaxies near the line-of-sight, so we can compare the observed number of absorption systems to that predicted by a simple model with a constant covering factor in Mg II absorbing gas within a maximum radius of each detected galaxy. The model is consistent with a covering factor of unity, but allowing for incompleteness in the detection of galaxies, the covering factor is less than unity. The redshifts of the galaxies are required to confirm this result.

1. INTRODUCTION

Two main hypotheses have been proposed to describe the metal-rich absorption systems in quasar spectra. The first, proposed by Bahcall & Spitzer (1969), suggests that the metal absorption systems arise in the halos of intervening galaxies. The halos are postulated to be spherical, and to have a covering factor in observable absorption of order unity. The second hypothesis which has been described by York (1988), suggests that the absorption arises in condensations associated with galaxies, but not necessarily part of the gravitationally bound halo of the luminous galaxy.

The second model is supported by observations that suggest the absorption systems are larger than normal galaxies. If the observed frequency of absorption systems is used to predict the halo sizes in the first model, radii of $\sim 50h^{-1}$ kpc are obtained (Bergeron & Boissé 1991; hereafter referred to as BB91), larger than either the optical or radio extent of normal galaxies. In addition, redshifts of absorption systems appear to be correlated on scales up ~ 600 km s^{-1} (Petitjean & Bergeron 1990), which is substantially larger than would be predicted for a population of absorbers in a single galactic halo. Metal absorption lines in our own galaxy's halo have a velocity dispersion of $\lesssim 200$ km s^{-1} (Vidal-Madjar *et al.* 1987; see also Savage *et al.* 1993).

The most direct approach to identifying the absorption systems is to study absorption systems for which both direct-image and spectroscopic data can be obtained. Ground-based studies are limited to the Mg II absorption regions in the redshift range $0.15 < z \lesssim 0.7$, the lower limit given by UV absorption in the atmosphere and the upper limit by the limiting magnitude at which galaxies might be imaged by a CCD. Typically one such absorption system is found over the full path to a typical quasar at $z = 2$ (Thomas & Webster 1990). Bergeron (1988; see also BB91) has undertaken the most extensive search for galaxies which are at similar redshifts to known low redshift Mg II absorption systems, and are close to the line-of-sight to the quasar. Bergeron finds that in most cases (12 out of 16, using the more recent compilations given by Lanzetta & Bowen 1990) a galaxy is found near the line-of-sight to the quasar with a similar velocity to the Mg II absorption line. Unfortunately many of the details of this study have not been

 0004-6256/93/106(3)/848/21/$0.90

published and the redshifts of other galaxies in the region are not available.

A further possibility is that some bright quasars might be gravitationally lensed, and thus overrepresented in the samples which have bright limiting magnitudes (Thomas & Webster 1990; Nottale 1988). All quasars chosen for absorption line studies are bright; thus the sample might be biased to include lensed quasars, which might preferentially intercept galaxies and show absorption lines. The observations described here will be used in a companion paper (Paper II; in preparation) to consider the possibility that some fraction of the quasars in the sample might be lensed.

In this work we have imaged quasars from several recent compilations of Mg II absorption lines to search for close galaxies. The important characteristics of our sample are its large size and the selection which is not biased with respect to the presence of close galaxies. The quasars were selected without considering the detection of absorption lines, since those without absorption systems provide an important control sample. Galaxies detected near the quasars will be observed spectroscopically at a later date so that redshifts can be determined. The complete sample enables the following questions to be considered.

(1) Are all absorption lines associated with a visible galaxy?

(2) Do all visible galaxies give rise to observable absorption?

In Sec. 2, the observations and initial data reduction are described. In Sec. 3 a catalogue of objects close to the quasars is presented. The distribution of galaxies near the quasars displaying Mg II absorption is considered in Sec. 4. In Sec. 5 we consider quasars which do not have Mg II absorption detected, but which do have close galaxies. A subsample of low redshift quasars is discussed in Sec. 6 and all the results are summarized in Sec. 7. We use a Hubble constant of $H_0=100h^{-1}$ km s^{-1} Mpc^{-1} and density parameter of $\Omega_0=1$ throughout.

2. OBSERVATIONS AND DATA REDUCTION

2.1 Selection of Quasars

The Mg II absorption lines, which have rest wavelengths of 2795.5 and 2802.7 Å, are spectroscopically observable in the optical bandpass for objects with redshifts of $0.15 \lesssim z \lesssim 2.5$. The requirement that the absorbing object be directly observable places an upper limit of $z \lesssim 0.7$ if the object is a galaxy with luminosity L_*, since the limiting magnitude for the CCD data is $m_R \sim 22$ (see discussion in Sec. 4). The quasars chosen for observation are listed in Table 1. These were selected from the published samples of quasars with intermediate ($\sim$5 Å) resolution spectra listed in Table 2 that satisfied the following criteria.

(1) $z_q < 2.5$, where z_q is the quasar redshift. This condition ensures that there is some wavelength range longward of the Lyman-α emission, where low redshift Mg II absorbing systems might be detected.

(2) $z_1 < 0.5$, where z_1 is the minimum redshift at which Mg II absorption could be detected in the published spectrum. This is to ensure a reasonable probability that galaxies at the absorption redshift could be detected in our CCD images.

(3) Constraints on right ascension and declination imposed by the allocated observing time and the location of the observatory (latitude +45.46° so declination > −10°).

Quasars satisfying these criteria, but near very bright stars, were not included in the sample, since we were unable to obtain sufficiently deep CCD frames to make the analysis worthwhile.

The selected quasars are listed in Table 1 with coordinates, V magnitudes, and redshifts from Hewitt & Burbidge (1987, 1989) as well as details of the spectroscopic observations and detections—if any—of Mg II absorption from the references in Table 2. The absorption system at redshift $z_{abs}=0.21$ in quasar 1148+387 reported by Boulade *et al.* (1987) has not been included because of its nondetection by Steidel & Sargent (1992). We note that recent observations with the Anglo-Australian Telescope (Drinkwater 1993) have revealed an error in the catalogue position of quasar 1228+078 which is corrected in this table.

2.2 Observations

Broadband R CCD images of the quasars were obtained using the 1.6 m telescope at the Observatoire Astronomique du Mont Mégantic. The observatory is situated in the south of Québec Province, Canada at a latitude of +45.46° and an elevation of 1114 m. An RCA CCD was used having a scale of 0.48 arcsec per pixel giving a field of 2.6 by 4.1 arcmin. The observations were made during a total of five observing sessions from 1989 June to 1991 April. A complete summary of the observations is incorporated in Table 1. For each object, the total exposure time was up to 2400 s in R, in three separate exposures. The conditions were generally close to photometric, except for two especially poor nights; these are noted in Table 1. The limiting magnitude varies significantly between images because of large, temperature-dependent variations in seeing. For instance, during the 1990 March run the ambient night temperature varied between −5 and −20 C, with the poorest seeing on nights when the temperature was falling rapidly.

2.3 Reduction

The images were corrected for zero level bias and the effects of charge skimming by subtracting a "cosmetic" bias frame from each image as described by Drinkwater & Hardy (1991). Variations in sensitivity across the field were removed by dividing the images by dome flats which had been corrected for nonuniform illumination by sky flats taken in twilight. This and subsequent treatment of the data was done using the IRAF[1] image analysis software.

[1]IRAF is distributed by the National Optical Astronomy Observatories, which is operated by the Association of Universities for Research in Astronomy, Inc. (AURA) under cooperative agreement with the National Science Foundation.

TABLE 1. Quasars observed.

QSO (1)	type (2)	RA (3)	(1950) Dec (4)	m_V (5)	z_{qso} (6)	z_1 (7)	z_2 (8)	z_{abs1} (9)	z_{abs2} (10)	ref (11)	date (12)	exp (13)	fwhm (14)	m_R (15)	phot (16)	m_{lim} (17)
0710+118	RX	7:10:15.38	11:51:23.9	16.60	0.768	0.47	0.76	-	-	1	15/04/91	2100	2.00	16.09	X	21.53
0736−063	R	7:36:30.20	−6:20:02.9	18.50	1.914	0.26	0.80	-	-	2	17/03/91	1800	2.16	16.65	D	21.79
0738+313	RX	7:38:00.18	31:19:01.8	16.14	0.631	0.11	0.41	0.2213	-	4	29/03/90	2400	2.50	16.47		21.91
0742+318	R	7:42:30.75	31:50:15.7	16.00	0.462	0.11	0.48	0.1917	-	4,6,(10)	30/03/90	2400	1.61	15.63		22.63
0835+580	RX	8:35:10.02	58:04:51.8	17.62	1.534	0.22	0.55	-	-	1a,3	28/03/90	2400	1.75	16.85		21.92
0836+195	R	8:36:15.00	19:32:24.6	17.60	1.691	0.22	0.54	-	-	1a,3	17/03/91	1902	2.23	17.22		22.23
0843+136	R	8:43:01.35	13:39:57.4	17.80	1.875	0.18	0.69	0.6054	0.6073	1,3	26/03/90	2500	1.89	17.11		21.93
0848+163	C	8:48:53.70	16:23:39.8	16.90	1.925	0.27	0.72	0.5862	0.5903	(1,2,3),7	13/04/91	1800	2.16	17.35		22.17
0854+191	CR	8:54:36.54	19:07:00.5	17.60	1.896	0.24	0.68	-	-	1,3,7	13/04/91	1800	2.06	17.59		22.25
0856+170	CR	8:56:04.09	17:03:09.1	17.40	1.449	0.18	0.53	-	-	1,3	29/03/90	2400	2.27	17.77		22.02
0856+189	C	8:56:37.45	18:55:32.2	17.70	1.286	0.20	0.46	-	-	1	13/04/91	1800	1.81	17.67		21.99
0952+179	R	9:52:11.83	17:57:44.9	17.23	1.472	0.14	0.80	0.2377	-	1,3,9	18/03/91	1819	2.33	17.14		21.82
0955+326	RX	9:55:25.44	32:38:23.0	15.78	0.533	0.17	0.60	-	-	1	14/04/91	1800	2.02	15.92		21.94
0957+561	R	9:57:57.30	56:08:22.6	17.00	1.405	0.21	0.38	-	-	2	18/03/91	1800	2.16	16.63	D	22.14
0958+551	C	9:58:08.05	55:09:05.8	16.00	1.751	0.18	0.65	0.2413	-	(1),3,7	28/03/90	2400	1.80	15.95	e	22.50
1017+280	C	10:17:06.00	28:00:60.0	15.69	1.928	0.27	0.80	-	-	2,7	17/03/91	1800	2.21	15.69		22.25
1038+064	RX	10:38:40.87	6:25:58.6	16.81	1.270	0.18	0.80	0.4416	-	1,9	22/03/90	1800	2.51	16.19		21.45
1049+616	R	10:49:22.43	61:41:18.2	16.48	0.422	0.11	0.41	0.2251	0.3933	4	25/03/90	2400	2.44	16.28	D	21.88
1054−034	OXR	10:54:10.35	−3:24:38.7	18.00	2.115	0.29	0.80	-	-	2,7	26/03/90	2400	1.95	17.70		22.06
1055−045	OR	10:55:40.18	−4:34:08.5	17.79	1.428	0.17	0.57	-	-	1,3	30/03/90	2300	1.75	17.29	e	22.50
1103−006	R	11:03:58.07	−0:36:37.7	16.46	0.426	0.14	0.53	-	-	1	14/04/91	2400	2.38	16.30		21.86
1104+167	R	11:04:36.66	16:44:17.1	15.70	0.634	0.31	0.67	-	-	1	15/04/91	1800	1.72	16.06	X	21.92
1115+080	C	11:15:41.50	8:02:24.0	16.99	1.718	0.19	0.71	-	-	2,7	18/03/91	1800	2.28	15.74	D	22.29
1126+101	R	11:26:38.70	10:08:32.0	18.00	1.515	0.14	0.52	-	-	1,3	29/03/90	2400	2.61	16.94		21.91
1127−145	RX	11:27:35.72	−14:32:54.7	16.90	1.187	0.17	0.42	0.3130	-	8	22/03/90	1800	2.50	16.74		21.32
1138+040	C	11:38:42.40	4:03:38.0	16.05	1.877	0.34	0.76	-	-	7	18/03/91	1800	2.53	16.84		22.18
1148−001	R	11:48:10.17	−0:07:13.1	17.34	1.982	0.23	0.76	-	-	2,7	18/03/91	1800	2.53	16.95		22.09
1148+387	R	11:48:53.27	38:42:34.2	17.04	1.303	0.11	0.80	0.5533	-	9	28/03/90	2400	1.87	16.84		22.52
1209+107	O	12:09:08.40	10:46:58.0	17.76	2.191	0.29	0.80	0.3930	0.6295	2	30/03/90	2331	1.50	17.62		22.26
1211+334	R	12:11:32.60	33:26:18.0	17.89	1.598	0.19	0.57	-	-	1,3	30/03/90	2400	1.53	17.36		22.20
1215+113	R	12:15:53.31	11:21:44.6	16.86	1.396	0.21	0.53	-	-	1	14/04/91	1800	2.26	16.67		21.98
1225+317	RX	12:25:55.94	31:45:12.6	15.87	2.219	0.29	0.80	-	-	2	17/03/91	1800	2.16	15.49	e	22.26
1228+078	O	12:28:01.62	7:49:39.2	17.47	1.813	0.22	0.71	-	-	2	17/03/91	1800	2.27	17.31		21.92
1246−057	O	12:46:38.80	−5:42:58.3	16.73	2.236	0.43	0.80	0.6399	-	2,9	18/03/91	1800	2.59	16.10	e	22.11
1246+377	C	12:46:28.74	37:46:49.7	16.98	1.242	0.14	0.80	-	-	1,9	14/04/91	1800	2.35	16.89	e	22.19
1256+357	CXR	12:56:07.84	35:44:53.7	17.96	1.882	0.24	0.67	-	-	1,3	30/03/90	2400	1.71	17.62	e	22.20
1257+346	CR	12:57:26.68	34:39:31.4	16.79	1.375	0.14	0.80	-	-	1,9	14/04/91	1800	2.56	16.38	e	22.22
1258+286	C	12:58:23.80	28:39:28.0	17.75	1.922	0.24	0.71	-	-	1,3	18/03/91	1800	2.67	17.28		21.97
1303+308	C	13:03:32.03	30:48:55.2	17.85	1.759	0.29	0.53	-	-	1	14/04/91	1800	2.62	17.21		22.26
1308+182	R	13:08:29.47	18:15:33.8	17.50	1.677	0.21	0.62	-	-	1,3	30/03/90	2400	1.93	18.45		22.57
1309−056	OX	13:09:00.74	−5:36:43.4	17.44	2.224	0.29	0.80	-	-	2	18/03/91	1917	2.46	17.22		22.08
1309+340	C	13:09:16.86	34:02:44.5	17.43	1.035	0.32	0.60	-	-	1	17/03/91	1800	1.78	17.29		22.70
1317+277	C	13:17:34.24	27:43:52.0	15.98	1.022	0.22	0.80	0.2887	0.6596	(1),9	15/04/91	1800	1.91	16.11	Xe	21.90
1318+29a	CX	13:18:53.65	29:03:30.3	16.90	1.703	0.27	0.61	-	-	1,3	18/03/91	1800	2.37	17.10		22.08
1318+29b	C	13:18:54.78	29:03:00.6	16.40	0.549	0.32	0.66	-	-	1	18/03/91	1800	2.24	16.29		22.08
1329+412	C	13:29:29.90	41:17:23.0	16.30	1.935	0.34	0.76	0.5009	-	7	26/03/90	2400	1.69	17.01		22.12
1331+170	RX	13:31:10.10	17:04:26.0	16.71	2.081	0.19	0.76	0.7443	0.7454	2,7	18/03/91	1800	2.47	16.43		22.29
1332+552	R	13:32:15.83	55:16:45.6	16.00	1.249	0.22	0.53	0.3740	-	5	22/03/90	1800	2.59	18.03		21.16
1346−036	O	13:46:08.25	−3:38:30.5	17.27	2.344	0.36	0.80	-	-	2	17/03/91	1800	1.95	16.83		22.37
1354+195	R	13:54:42.08	19:33:43.9	16.02	0.720	0.22	0.80	0.4564	-	1,9,10a	26/03/90	2400	1.98	16.28		22.19
1416+067	RX	14:16:38.78	6:42:20.9	16.79	1.436	0.14	0.53	-	-	1,3	17/03/91	1800	1.93	16.41		22.54
1416+159	R	14:16:27.67	15:54:52.1	17.75	1.472	0.24	0.59	-	-	1	14/04/91	1800	2.42	17.72		22.06
1421+122	R	14:21:04.69	12:13:26.7	18.04	1.611	0.22	0.71	-	-	2	17/03/91	1800	1.85	17.91		22.39
1421+330	C	14:21:17.52	33:05:55.5	16.70	1.904	0.24	0.69	0.4566	-	1,3	30/03/90	2400	1.82	15.97	e	22.09
1435+638	R	14:35:37.20	63:49:36.0	15.00	2.068	0.34	0.76	-	-	7	22/03/90	1800	2.05	16.07		21.53
1511+103	R	15:11:04.56	10:22:15.2	17.73	1.546	0.18	0.53	0.4369	-	(1a),3	25/06/89	1500	2.65	16.72		21.08
1512+370	RX	15:12:46.87	37:01:55.2	15.50	0.371	0.28	0.39	-	-	6	01/07/89	900	1.92	16.13	X	21.29
1517+239	C	15:17:08.19	23:56:52.6	16.40	1.898	0.22	0.76	0.7382	-	1,2,3,7	14/04/91	1800	2.69	17.46		21.85
1556+335	RX	15:56:59.43	33:31:47.4	17.00	1.646	0.14	0.57	-	-	1,3	01/07/89	1500	1.89	17.20	X	21.98
1559+173	R	15:59:04.63	17:22:36.5	17.70	1.944	0.34	0.69	-	-	1,3	26/03/90	2400	2.06	18.10		22.28
1602−001	R	16:02:22.11	−0:11:00.2	17.49	1.625	0.25	0.71	-	-	2	26/03/90	2400	2.15	17.16		22.25
1634+176	R	16:34:02.73	17:41:10.1	18.00	1.897	0.25	0.68	-	-	1a,3	01/07/89	1500	1.76	18.46		22.15
1634+706	CX	16:34:51.70	70:37:37.0	14.90	1.334	0.22	0.80	0.6694	-	9	26/06/89	1376	1.86	13.68	e	21.66
1641+399	RX	16:41:17.62	39:54:10.7	15.96	0.595	0.25	0.68	-	-	1a,6,10	01/07/89	1500	1.76	17.33	X	22.05
1704+608	RX	17:04:03.47	60:48:31.1	15.28	0.371	0.11	0.41	0.1634	0.2219	4,6	25/06/89	1500	2.43	14.83		21.05
1715+535	C	17:15:30.70	53:31:24.0	16.30	1.929	0.34	0.76	0.3673	-	7	26/06/89	1500	1.72	15.30	D	21.80
1756+237	RX	17:56:56.50	23:43:55.0	18.00	1.721	0.16	0.62	0.3713	-	(1),3	25/06/89	1500	2.49	16.30	D	21.18
1828+487	RX	18:28:13.55	48:42:40.4	16.81	0.692	0.25	0.71	-	-	1	14/04/91	1800	2.92	16.59		21.96
2120+168	RX	21:20:25.53	16:51:46.4	17.96	1.805	0.27	0.62	-	-	1,3	26/06/89	1500	2.22	17.40		21.57
2145+067	RX	21:45:36.11	6:43:41.2	16.47	0.990	0.22	0.80	0.7905	-	(1),7,9	30/06/89	900	2.84	15.40		20.93
2230+114	RX	22:30:07.84	11:28:22.8	17.33	1.037	0.44	0.87	-	-	7	17/12/90	2400	2.08	16.63		22.65

Notes to TABLE 1

1: quasar name, 2: detection technique (C; color, O; spectral survey, R; radio, X; X-ray), 3,4: R.A. and Dec. (1950.0), 5: quasar *V* magnitude, 6: quasar redshift (1–6 from Hewitt & Burbidge 1987, 1989), 7,8: the minimum and maximum redshifts at which Mg II might be observed in the published spectra, 9,10: redshifts of any Mg II absorption systems, 11: reference for the published spectra, parentheses signifying a nondetection (see Table 2), 12: date observed (UT), 13: exposure time (s), 14: FWHM seeing (arcsec), 15: quasar *R* magnitude, 16: photometry flag (blank; photometric, *X*; not photometric, D; double image with magnitude from DAOPHOT, e; no DAOPHOT fitting was possible), 17: limiting *R* magnitude of image (the magnitude of the faintest object for which the formal error in the magnitude was less than 0.2 mag).

TABLE 2. Mg II Absorption system references.

number	reference	W_{rest}(Å)
1	Weyman *et al.* (1979)	≈ 0.5
1a	Weyman *et al.* (1979)	≈ 0.8
2	Young, *et al.* (1982)	0.6
3	Foltz *et al.* (1986)	0.5
4	Boulade *et al.* (1987)	–
5	Miller *et al.* (1987)	–
6	Tytler *et al.* (1987)	≈ 0.4
7	Sargent *et al.* (1988)	0.3
8	Bergeron & Boissé (1991)	≈ 0.5
9	Steidel & Sargent (1992)	0.3
10	Bechtold & Ellingson (1992)	0.3
10a	Bechtold & Ellingson (1992)	0.6

Notes to TABLE 2
W_{rest} is the rest equivalent width limit for each sample.

The three images taken of each object were combined using a sigma-clipping algorithm to remove spurious signals due to cosmic rays. The effective resolution of the final image (atmospheric seeing convolved with tracking errors) was measured by fitting Gaussians to about eight stars in the field and taking the mean value of the corresponding full width at half-maximum (FWHM). The values are given in Table 1. Any images with FWHM greater than 3 arcsec for stellar images were discarded.

Flux calibrations were made each night from observations of the standard fields of Christian *et al.* (1985); no color corrections were needed for the *R* filter. To correct for atmospheric extinction we adopted coefficients provided for the Anglo-Australian Observatory, which is at a similar altitude to Mont Mégantic since coefficients were not available for the latter. The value used was 0.094 *R* mag per airmass (Roy 1990). The *R* magnitudes of all the QSOs were measured and are given in Table 1. The magnitudes were calculated by summing the flux above sky in fixed apertures of 5 arcsec radius, except when there was a close bright companion. In those cases, the magnitude is derived from the point spread function (PSF) fitting stage of the DAOPHOT analysis (see below), and the photometry is flagged "D" in Table 1.

3. IMAGE ANALYSIS

3.1 Image Detection

The image analysis was primarily undertaken using the FOCAS (faint object classification and analysis system) package in IRAF (Valdes 1982a). First a catalogue of objects was determined. Relatively conservative limits were used to determine the catalogue, each image having greater than 16 pixels $3\sigma_{sky}$ above the background. Fainter images could be detected, but star–galaxy classification algorithms become much less efficient at faint magnitudes. Merged images were identified, and each catalogue was carefully checked by eye for any image detections that were clearly spurious. Images which were saturated or on the boundary of the frame were not included in the final catalogue. Table 3 lists all objects found within 30 arcsec of each quasar in the FOCAS catalogues.

Within FOCAS, two parameters are traditionally used to distinguish between stars and galaxies—scale and fraction. Initially a stellar PSF is constructed from stellar images not merged with any other objects. A number of templates are then constructed with Gaussian dispersions which are some fixed multiple of the standard PSF (Valdes 1982b). The template which best fits the image is then selected and the scale of the image thereby determined. Since such models provide poor fits to galaxies, a two-component fit can be made, whereby some fraction of the image is fitted with stellar template and the remainder is fitted with a broadened Gaussian (Valdes 1982b).

We investigated the power of both scale and fraction compared to other algorithms for star–galaxy separation in our data, for example those used by the Automatic Plate Measuring facility (Maddox *et al.* 1990). The quasar was excluded from the images used to generate the PSF. We found that the scale parameter was as efficient as other methods for correctly discriminating stars from galaxies, and that the use of the fraction parameter did not substantially change the classifications. We chose to call those objects with scale 0.7–1.2 stars and those with scale 1.2–10.0 galaxies. The few images with scales outside these ranges were almost invariably noise. In addition, we discriminated between bright and faint images in the catalogue at a fixed instrumental magnitude, typically corresponding to $m_R \sim 20$. Classifications of the faint images are much less certain, and these are denoted "faint star" or "faint galaxy" in the final catalogue.

3.2 Photometry and Magnitude Limits

The simple threshold detection used in FOCAS does not produce lists with well-defined magnitude limits. A more robust approach is described by Harris (1990) who defines a "reasonable" limiting magnitude as the magnitude at which the fraction of objects detected drops to 0.5 (Harris *et al.* 1991). Ideally this would be determined empirically by adding artificial stars to the data and measuring the fraction detected as a function of magnitude. A simpler approach can be used, based on the fact that this corresponds to cutting of the image detection at a given signal-to-noise ratio (SNR). This means that if we specify a sufficiently high SNR cutoff, we can then estimate the magnitude limit from the magnitudes of the stars at this SNR as described below.

If the intensity of a star is measured in an aperture of radius *r* arcsec, the SNR ratio of the measurement is

$$\mathrm{SNR} = \frac{I(r)}{\sqrt{n\sigma_s}},$$

where $I(r)$ is the intensity within a radius r, n is the number of pixels in the aperture, and σ_s^2 the variance of the sky background noise. For a Gaussian profile, the SNR is greatest for $r_0 = 1.6\rho$ where ρ is the Gaussian sigma of the image profile (Pritchet & Kline 1981). We adopted a ra-

TABLE 3. Catalogue of quasar companions.

δRA	δDec	r	cls	m_R	Δm_R	δRA	δDec	r	cls	m_R	Δm_R
QSO 0710+118, $z = 0.768$, seeing=2.0 arcsec, magnitude limit=21.53											
-25.5	-13.3	28.7	g	19.23	0.02	6.1	6.4	8.8	s	15.90	0.00
-21.9	10.0	24.0	s	19.59	0.03	6.7	7.6	10.2	s	14.57	0.00
-15.6	22.2	27.2	fg	21.49	0.17	12.9	-16.8	21.2	fg	21.44	0.18
-4.8	-10.7	11.8	s	18.80	0.02	17.5	16.3	23.9	s	19.02	0.02
-4.2	-19.2	19.6	fs	21.24	0.15	18.4	0.3	18.4	s	20.91	0.12
0.0	0.0	0.0	s	16.09	0.00	18.9	-6.8	20.0	s	18.83	0.02
1.2	16.2	16.2	s	19.52	0.04	21.1	-4.6	21.6	fs	21.04	0.12
3.9	-6.8	7.9	s	18.51	0.01	28.0	-0.9	28.0	s	20.13	0.05
5.2	-0.9	5.3	s	15.93	0.00						
QSO 0736−063, $z = 1.914$, seeing=2.4 arcsec, magnitude limit=21.79											
-24.2	0.4	24.2	fg	21.37	0.15	0.0	0.0	0.0	s	16.65	0.00
-22.6	0.2	22.6	fg	21.44	0.16	2.9	29.4	29.5	fs	21.35	0.15
-18.9	-11.4	22.1	s	20.55	0.06	10.2	-6.9	12.4	s	20.41	0.07
-10.9	21.2	23.8	s	17.10	0.00	10.3	15.9	18.9	fs	21.60	0.16
-10.4	5.0	11.6	g	20.85	0.09	15.0	-8.4	17.2	fs	21.42	0.15
-6.4	-22.3	23.2	s	20.83	0.08	17.0	1.0	17.0	fg	21.49	0.17
-5.7	2.0	6.0	s	17.89	0.01	19.3	-16.2	25.2	fg	21.53	0.17
-2.9	7.5	8.0	fg	21.45	0.17	19.4	-10.2	21.9	s	20.22	0.05
-1.6	-3.8	4.1	g	20.41	0.20	19.9	0.8	19.9	s	21.13	0.12
QSO 0738+313, $z = 0.631$, seeing=2.8 arcsec, magnitude limit=21.91											
-27.1	-9.6	28.7	g	19.70	0.03	0.0	0.0	0.0	s	16.47	0.00
-12.9	6.2	14.3	s	16.57	0.00	1.9	-5.5	5.8	fs	20.44	0.20
-7.9	9.8	12.6	fs	20.13	0.04	2.1	1.5	2.6	fg	20.93	0.20
-6.0	4.1	7.2	fg	21.11	0.12	3.4	-19.8	20.0	s	18.32	0.01
-2.4	9.2	9.5	fg	21.52	0.16	5.2	24.3	24.8	s	17.39	0.00
-1.0	11.5	11.5	s	20.44	0.06						
QSO 0742+318, $z = 0.462$, seeing=1.6 arcsec, magnitude limit=22.63											
-23.4	-5.3	24.0	s	16.25	0.00	7.0	23.6	24.6	s	18.60	0.01
-13.8	-10.7	17.5	s	15.97	0.00	8.0	10.3	13.1	s	17.20	0.00
-9.6	-10.6	14.4	g	20.45	0.04	8.9	-17.6	19.7	fg	22.37	0.17
-8.4	18.3	20.1	fg	22.04	0.12	16.0	-20.6	26.1	g	20.61	0.04
-3.5	3.6	5.0	fs	20.67	0.20	18.5	15.0	23.8	fs	21.97	0.12
0.0	0.0	0.0	s	15.63	0.00						
QSO 0835+580, $z = 1.534$, seeing=1.7 arcsec, magnitude limit=21.92											
0.0	0.0	0.0	s	16.85	0.00	4.3	21.9	22.3	fs	21.66	0.15
2.8	-20.0	20.2	s	17.84	0.01	9.0	0.4	9.0	g	21.10	0.10
3.0	1.5	3.3	fs	21.73	0.20	11.5	-18.4	21.7	s	20.02	0.04
3.3	6.1	6.9	fg	21.57	0.15						
QSO 0836+195, $z = 1.691$, seeing=2.4 arcsec, magnitude limit=22.23											
-21.3	-14.8	26.0	fs	21.95	0.14	0.1	-16.3	16.3	s	19.39	0.01
0.0	0.0	0.0	s	17.22	0.00	10.4	1.1	10.4	fg	22.04	0.16
QSO 0843+136, $z = 1.875$, seeing=1.8 arcsec, magnitude limit=21.93											
-22.3	3.6	22.6	s	21.87	0.19	4.0	-26.5	26.8	g	20.36	0.05
-18.9	5.3	19.6	g	19.64	0.03	10.9	11.7	16.0	g	20.18	0.04
-6.2	23.3	24.1	g	20.76	0.07	15.1	-5.2	15.9	s	15.78	0.00
0.0	0.0	0.0	s	17.11	0.00	29.9	-1.3	29.9	g	21.68	0.17
QSO 0848+163, $z = 1.925$, seeing=2.1 arcsec, magnitude limit=22.17											
-13.4	-11.9	17.9	s	18.17	0.01	2.4	-16.2	16.3	g	19.64	0.02
-6.6	-27.3	28.1	g	21.68	0.14	8.8	19.9	21.8	fg	22.12	0.18
0.0	0.0	0.0	s	17.35	0.00						

TABLE 3. (continued)

δRA	δDec	r	cls	m_R	Δm_R	δRA	δDec	r	cls	m_R	Δm_R
QSO 0854+191, $z = 1.896$, seeing=2.0 arcsec, magnitude limit=22.25											
-17.4	-11.4	20.8	fs	22.18	0.19	0.0	0.0	0.0	s	17.59	0.00
-4.0	-23.4	23.7	fs	22.25	0.19	12.8	-1.9	13.0	g	21.46	0.10
QSO 0856+170, $z = 1.449$, seeing=2.5 arcsec, magnitude limit=22.02											
-10.4	0.8	10.5	g	21.42	0.15	10.2	10.6	14.8	s	15.97	0.00
-9.6	11.6	15.1	g	18.52	0.01	13.0	-14.0	19.1	s	16.24	0.00
0.0	0.0	0.0	s	17.77	0.01						
QSO 0856+189, $z = 1.286$, seeing=1.8 arcsec, magnitude limit=21.99											
0.0	0.0	0.0	s	17.67	0.00	29.5	-2.4	29.6	fs	21.97	0.19
QSO 0952+179, $z = 1.472$, seeing=2.3 arcsec, magnitude limit=21.82											
-24.2	-17.4	29.7	fs	21.89	0.20	9.5	9.5	13.4	s	19.45	0.02
-11.5	-19.9	23.0	g	20.95	0.09	21.6	10.7	24.1	s	21.00	0.09
-3.5	-26.0	26.3	s	20.89	0.08	25.8	-2.7	26.0	fg	20.63	0.06
0.0	0.0	0.0	s	17.14	0.00	26.3	-0.2	26.3	g	20.56	0.06
QSO 0955+326, $z = 0.533$, seeing=2.0 arcsec, magnitude limit=21.94											
-26.0	-5.0	26.5	fg	21.94	0.20	0.0	0.0	0.0	s	15.92	0.00
-12.0	-24.8	27.5	fg	21.70	0.16	19.2	18.3	26.5	g	21.50	0.13
QSO 0957+561, $z = 1.405$, seeing=2.1 arcsec, magnitude limit=22.14											
-26.8	8.2	28.1	s	18.51	0.01	1.8	15.3	15.4	s	20.49	0.05
-7.3	-5.7	9.2	fg	20.74	0.10	7.2	3.0	7.8	g	19.72	0.05
-1.3	5.9	6.0	s	16.94	0.00	11.0	-2.3	11.2	g	20.77	0.08
-0.4	-24.4	24.4	s	18.22	0.01	11.1	5.5	12.4	fg	21.36	0.11
0.0	0.0	0.0	s	16.63	0.00	22.4	-7.6	23.7	g	20.75	0.05
1.0	1.8	2.0	g	18.71	0.00	25.0	14.5	28.9	s	21.01	0.07
1.2	26.0	26.0	s	20.02	0.03						
QSO 0958+551, $z = 1.751$, seeing=1.7 arcsec, magnitude limit=22.50											
-8.7	21.8	23.4	g	19.34	0.01	9.7	-14.8	17.7	fg	21.93	0.12
0.0	0.0	0.0	s	15.95	0.00						
QSO 1017+280, $z = 1.928$, seeing=2.2 arcsec, magnitude limit=22.25											
-2.4	22.7	22.8	fs	22.06	0.17	5.9	-18.3	19.3	g	21.03	0.07
0.0	0.0	0.0	s	15.69	0.00	6.1	25.9	26.6	s	20.65	0.05
0.5	-18.3	18.3	g	20.51	0.04						
QSO 1038+064, $z = 1.270$, seeing=2.8 arcsec, magnitude limit=21.45											
-8.1	7.9	11.3	s	16.43	0.00	9.6	1.7	9.7	g	20.83	0.14
-1.5	7.2	7.3	fg	20.59	0.11	9.6	24.9	26.7	fg	21.11	0.16
0.0	0.0	0.0	s	16.19	0.00	13.9	15.1	20.5	g	19.01	0.02
QSO 1049+616, $z = 0.422$, seeing=2.7 arcsec, magnitude limit=21.88											
0.0	0.0	0.0	s	16.28	0.00	14.6	11.9	18.9	s	21.30	0.10
1.9	2.2	2.9	g	19.11	0.00	22.0	3.7	22.3	fg	21.62	0.13
QSO 1054−034, $z = 2.115$, seeing=2.0 arcsec, magnitude limit=22.06											
-17.1	-3.1	17.4	g	21.17	0.08	0.0	0.0	0.0	s	17.70	0.00
-4.8	3.0	5.7	g	19.81	0.02						
QSO 1055−045, $z = 1.428$, seeing=1.7 arcsec, magnitude limit=22.50											
-2.0	19.4	19.5	s	20.94	0.05	15.0	12.1	19.3	s	20.99	0.05
0.0	0.0	0.0	s	17.29	0.00	19.6	-1.7	19.6	s	18.32	0.01
9.5	-24.3	26.1	s	20.77	0.04	22.1	-5.7	22.8	s	20.70	0.04
QSO 1103−006, $z = 0.426$, seeing=2.3 arcsec, magnitude limit=21.86											
-26.6	-7.9	27.7	g	21.29	0.12	9.8	10.6	14.5	s	17.31	0.00
-16.7	10.2	19.6	s	18.62	0.01	10.1	-27.9	29.7	s	19.88	0.03
-14.4	-4.3	15.0	g	19.64	0.03	15.9	-13.6	20.9	g	20.57	0.05
0.0	0.0	0.0	s	16.30	0.00						

TABLE 3. (continued)

δRA	δDec	r	cls	m_R	Δm_R	δRA	δDec	r	cls	m_R	Δm_R
QSO 1104+167, $z = 0.634$, seeing=1.7 arcsec, magnitude limit=21.92											
-14.1	-0.5	14.1	fg	21.75	0.19	4.0	16.9	17.3	g	20.78	0.07
-13.1	19.4	23.4	fs	21.92	0.18	6.7	13.7	15.2	g	20.96	0.08
-12.3	-22.9	26.0	fg	21.58	0.17	9.5	-26.0	27.7	g	21.31	0.12
0.0	0.0	0.0	s	16.06	0.00	16.7	-22.0	27.7	s	20.90	0.08
QSO 1115+080, $z = 1.718$, seeing=2.2 arcsec, magnitude limit=22.29											
-20.7	-10.8	23.4	g	19.28	0.01	0.0	0.0	0.0	s	15.74	0.00
-14.9	-11.7	18.9	g	20.80	0.06	5.6	-21.8	22.5	s	18.97	0.01
-12.4	-0.9	12.4	g	20.30	0.04	16.4	9.6	19.0	fg	21.54	0.10
-1.4	1.5	2.1	s	17.62	0.00	23.9	-0.5	23.9	fg	21.60	0.10
QSO 1126+101, $z = 1.515$, seeing=3.0 arcsec, magnitude limit=21.91											
0.0	0.0	0.0	s	16.94	0.00	4.4	8.7	9.7	fg	20.01	0.06
4.2	6.4	7.7	fg	20.51	0.06	5.6	8.7	10.3	fg	20.51	0.06
QSO 1127−145, $z = 1.187$, seeing=2.8 arcsec, magnitude limit=21.32											
-7.5	20.7	22.0	s	18.76	0.02	7.2	15.7	17.2	g	20.12	0.07
0.0	0.0	0.0	s	16.74	0.00	8.7	3.7	9.4	g	20.05	0.07
0.7	19.1	19.1	g	19.64	0.04	20.8	-1.1	20.8	g	20.57	0.10
QSO 1138+040, $z = 1.877$, seeing=2.5 arcsec, magnitude limit=22.18											
0.0	0.0	0.0	s	16.84	0.00	12.9	-11.5	17.3	g	21.20	0.08
2.4	-13.0	13.2	s	16.16	0.00						
QSO 1148−001, $z = 1.982$, seeing=2.7 arcsec, magnitude limit=22.09											
-29.1	4.6	29.5	g	20.91	0.07	0.0	0.0	0.0	s	16.95	0.00
-11.2	10.0	15.1	s	20.57	0.05	26.8	-8.9	28.3	fs	22.01	0.18
-3.8	-12.4	13.0	s	21.12	0.09						
QSO 1148+387, $z = 1.303$, seeing=1.8 arcsec, magnitude limit=22.52											
-16.6	-17.7	24.3	g	19.12	0.01	16.2	14.6	21.8	s	20.03	0.02
-4.0	-2.7	4.8	fs	22.52	0.19	19.9	-20.5	28.5	s	21.53	0.08
-2.7	-19.7	19.9	fs	22.24	0.14	23.3	10.5	25.5	fs	22.08	0.13
-0.5	3.3	3.3	fg	21.00	0.20	24.0	-3.8	24.3	fs	21.97	0.12
0.0	0.0	0.0	s	16.84	0.00	28.2	-8.9	29.6	g	22.08	0.13
15.6	-3.3	15.9	s	21.44	0.08						
QSO 1209+107, $z = 2.191$, seeing=1.4 arcsec, magnitude limit=22.26											
-19.9	-1.1	19.9	s	20.77	0.05	0.0	0.0	0.0	s	17.62	0.00
-8.5	17.3	19.3	s	21.13	0.07	5.1	5.0	7.1	g	21.57	0.11
-5.4	1.1	5.5	s	20.57	0.04						
QSO 1211+334, $z = 1.598$, seeing=1.6 arcsec, magnitude limit=22.20											
-20.4	8.0	21.9	g	21.48	0.09	17.8	4.0	18.2	s	18.05	0.00
0.0	0.0	0.0	s	17.36	0.00						
QSO 1215+113, $z = 1.396$, seeing=2.3 arcsec, magnitude limit=21.98											
-20.5	-3.5	20.8	s	17.16	0.00	-4.0	19.8	20.2	s	21.61	0.13
-11.1	-4.4	11.9	fs	21.77	0.16	0.0	0.0	0.0	s	16.67	0.00
QSO 1225+317, $z = 2.219$, seeing=2.1 arcsec, magnitude limit=22.26											
-26.1	11.7	28.6	g	21.79	0.11	4.4	14.7	15.3	s	18.89	0.01
-8.7	0.8	8.8	g	21.75	0.12	24.0	6.7	24.9	s	21.70	0.10
0.0	0.0	0.0	g	15.49	0.00						
QSO 1228+078, $z = 1.813$, seeing=2.3 arcsec, magnitude limit=21.92											
-18.1	-7.1	19.4	s	19.79	0.02	0.0	0.0	0.0	s	17.31	0.00
-8.5	14.5	16.8	s	20.95	0.07	10.9	-14.4	18.1	s	20.43	0.04
QSO 1246−057, $z = 2.236$, seeing=2.5 arcsec, magnitude limit=22.11											
-19.7	18.2	26.8	fs	21.76	0.14	1.7	-23.6	23.7	fs	21.62	0.13
0.0	0.0	0.0	s	16.10	0.00	12.2	11.7	16.9	s	19.93	0.03

TABLE 3. (continued)

δRA	δDec	r	cls	m_R	Δm_R	δRA	δDec	r	cls	m_R	Δm_R
QSO 1246+377, z = 1.242, seeing=2.3 arcsec, magnitude limit=22.19											
0.0	0.0	0.0	s	16.89	0.00	20.3	20.5	28.9	fs	21.96	0.15
6.0	-16.9	18.0	fs	22.19	0.19						
QSO 1256+357, z = 1.882, seeing=1.7 arcsec, magnitude limit=22.20											
-27.9	4.8	28.3	g	20.29	0.03	5.0	6.0	7.8	fg	22.03	0.13
-8.3	-17.7	19.6	g	21.61	0.09	15.0	-17.0	22.7	s	21.00	0.05
0.0	0.0	0.0	s	17.62	0.00						
QSO 1257+346, z = 1.375, seeing=2.5 arcsec, magnitude limit=22.22											
0.0	0.0	0.0	s	16.38	0.00	14.7	16.5	22.1	s	21.13	0.07
1.7	17.1	17.2	s	21.23	0.08						
QSO 1258+286, z = 1.922, seeing=2.5 arcsec, magnitude limit=21.97											
-14.7	20.7	25.4	fg	21.68	0.13	4.3	24.6	24.9	g	21.10	0.08
-6.5	-27.6	28.3	g	20.38	0.04	7.5	-15.5	17.2	s	15.93	0.00
0.0	0.0	0.0	s	17.28	0.00	13.9	18.4	23.1	s	19.04	0.01
QSO 1303+308, z = 1.759, seeing=2.6 arcsec, magnitude limit=22.26											
-23.1	12.6	26.3	fg	21.89	0.13	0.0	0.0	0.0	s	17.21	0.00
-13.7	-16.5	21.4	g	19.57	0.02	13.3	14.8	19.9	s	20.56	0.04
QSO 1308+182, z = 1.677, seeing=1.9 arcsec, magnitude limit=22.57											
-23.0	-10.7	25.4	fs	22.47	0.18	-0.6	14.3	14.3	fs	22.06	0.12
-11.8	-12.1	16.9	fs	22.01	0.12	0.0	0.0	0.0	s	18.45	0.01
-4.6	3.1	5.6	s	21.25	0.06	24.7	16.0	29.4	g	21.02	0.05
QSO 1309−056, z = 2.224, seeing=2.3 arcsec, magnitude limit=22.08											
-1.8	16.2	16.3	g	21.52	0.11	22.5	1.8	22.5	s	21.19	0.08
0.0	0.0	0.0	s	17.22	0.00						
QSO 1309+340, z = 1.035, seeing=1.7 arcsec, magnitude limit=22.70											
-21.4	18.1	28.1	s	20.47	0.03	0.6	-13.5	13.5	s	18.74	0.01
-2.4	4.8	5.4	fg	22.69	0.21	2.5	-6.7	7.2	g	20.92	0.06
0.0	0.0	0.0	s	17.29	0.00						
QSO 1317+277, z = 1.022, seeing=1.9 arcsec, magnitude limit=21.90											
-6.5	4.4	7.8	fg	21.87	0.20	0.0	0.0	0.0	s	16.11	0.00
QSO 1318+29a, z = 1.703, seeing=2.4 arcsec, magnitude limit=22.08											
0.0	0.0	0.0	s	17.10	0.00						
QSO 1318+29b, z = 0.549, seeing=2.4 arcsec, magnitude limit=22.08											
-3.5	-23.2	23.5	s	21.77	0.14	0.0	0.0	0.0	s	16.29	0.00
QSO 1329+412, z = 1.935, seeing=1.7 arcsec, magnitude limit=22.12											
-10.6	15.9	19.1	s	16.96	0.00	0.6	-2.4	2.4	fg	22.12	0.02
0.0	0.0	0.0	s	17.01	0.00						
QSO 1331+170, z = 2.081, seeing=2.4 arcsec, magnitude limit=22.29											
0.0	0.0	0.0	s	16.43	0.00	26.4	-7.8	27.6	g	20.95	0.06
17.6	-9.7	20.1	fs	21.68	0.12						
QSO 1332+552, z = 1.249, seeing=2.8 arcsec, magnitude limit=21.16											
-22.3	-6.5	23.2	fs	21.16	0.17	0.0	0.0	0.0	s	18.03	0.01
-10.9	-13.9	17.7	s	18.90	0.02	1.6	7.2	7.3	fg	21.12	0.17
-6.5	13.6	15.1	s	20.05	0.07	3.7	-21.1	21.4	s	20.60	0.10
-2.6	4.8	5.5	g	19.77	0.05	22.2	6.4	23.1	s	20.70	0.11
-1.0	13.5	13.5	fs	20.85	0.14						
QSO 1346−036, z = 2.344, seeing=2.0 arcsec, magnitude limit=22.37											
-18.9	22.1	29.0	s	21.60	0.09	6.4	-7.9	10.2	s	21.34	0.08
-10.7	17.6	20.6	fs	21.84	0.12	10.4	1.0	10.4	fs	21.99	0.15
-2.0	9.0	9.2	s	18.84	0.01	12.9	-23.8	27.1	fs	21.68	0.09
0.0	0.0	0.0	s	16.83	0.00	18.2	16.1	24.4	fs	21.71	0.10
1.1	25.2	25.3	g	21.53	0.09						

TABLE 3. (continued)

δRA	δDec	r	cls	m_R	Δm_R	δRA	δDec	r	cls	m_R	Δm_R
QSO 1354+195, $z = 0.720$, seeing=2.0 arcsec, magnitude limit=22.19											
-21.3	-11.8	24.3	g	21.15	0.07	1.2	7.6	7.7	g	21.38	0.09
-16.1	-22.8	27.9	fs	21.92	0.15	3.0	-6.3	7.0	fg	21.70	0.13
-11.0	16.9	20.2	g	21.25	0.08	25.9	-1.3	26.0	fs	22.09	0.18
0.0	0.0	0.0	s	16.28	0.00						
QSO 1416+067, $z = 1.436$, seeing=1.9 arcsec, magnitude limit=22.54											
-6.3	5.2	8.2	fg	21.95	0.11	0.0	0.0	0.0	s	16.41	0.00
-4.4	-13.9	14.5	s	16.62	0.00	10.8	-23.7	26.1	fs	22.46	0.17
QSO 1416+159, $z = 1.472$, seeing=2.4 arcsec, magnitude limit=22.06											
-22.1	3.8	22.5	g	20.87	0.06	0.0	0.0	0.0	s	17.72	0.00
-19.6	-5.9	20.5	fs	21.98	0.17	9.1	20.4	22.4	s	20.55	0.05
QSO 1421+122, $z = 1.611$, seeing=1.7 arcsec, magnitude limit=22.39											
0.0	0.0	0.0	s	17.91	0.00	10.4	-3.8	11.1	s	21.26	0.07
2.9	-6.0	6.7	s	20.05	0.03	16.7	-1.9	16.8	g	21.17	0.06
5.7	6.6	8.7	fs	22.03	0.14	20.0	2.1	20.1	fs	21.97	0.13
7.3	-11.4	13.6	g	21.31	0.08						
QSO 1421+330, $z = 1.904$, seeing=1.7 arcsec, magnitude limit=22.09											
-3.7	-5.2	6.4	g	21.79	0.16	0.0	0.0	0.0	s	15.97	0.00
QSO 1435+638, $z = 2.068$; seeing=2.1 arcsec, magnitude limit=21.53											
0.0	0.0	0.0	s	16.07	0.00	18.2	21.5	28.2	g	20.13	0.05
QSO 1511+103, $z = 1.546$, seeing=2.8 arcsec, magnitude limit=21.08											
-23.7	-7.8	24.9	fg	19.47	0.05	-4.5	20.5	21.0	s	19.30	0.04
-18.8	-7.8	20.3	s	17.05	0.01	0.0	0.0	0.0	s	16.72	0.00
-12.8	-19.5	23.4	g	19.50	0.05						
QSO 1512+370, $z = 0.371$, seeing=1.9 arcsec, magnitude limit=21.29											
-24.9	-11.4	27.4	s	20.89	0.14	0.0	0.0	0.0	s	16.13	0.00
-24.3	1.9	24.4	g	20.68	0.11	10.1	-2.8	10.5	g	19.89	0.06
-20.3	-11.2	23.2	g	20.62	0.10						
QSO 1517+239, $z = 1.898$, seeing=2.5 arcsec, magnitude limit=21.85											
0.0	0.0	0.0	s	17.46	0.00						
QSO 1556+335, $z = 1.646$, seeing=1.8 arcsec, magnitude limit=21.98											
-21.5	-6.7	22.5	g	21.04	0.09	0.0	14.9	14.9	fs	21.85	0.18
-14.7	5.7	15.7	fs	21.68	0.16	19.8	-21.6	29.3	g	20.20	0.04
0.0	0.0	0.0	s	17.20	0.00	20.4	-8.6	22.1	g	20.63	0.06
QSO 1559+173, $z = 1.944$, seeing=2.0 arcsec, magnitude limit=22.28											
-28.7	1.7	28.8	s	19.16	0.02	8.6	15.9	18.0	fs	22.10	0.16
-2.9	-3.3	4.4	fg	22.18	0.27	10.4	-11.7	15.7	s	18.41	0.01
-2.1	27.4	27.5	g	20.91	0.05	11.1	-17.1	20.4	s	21.47	0.10
0.0	0.0	0.0	s	18.10	0.01	25.5	11.5	28.0	s	17.07	0.00
QSO 1602−001, $z = 1.625$, seeing=2.2 arcsec, magnitude limit=22.25											
-17.9	6.6	19.1	s	17.54	0.00	3.7	-20.5	20.8	s	18.51	0.01
-6.8	3.8	7.7	s	19.27	0.02	12.9	-20.1	23.9	s	20.41	0.04
0.0	0.0	0.0	s	17.16	0.00	19.8	19.9	28.0	s	19.15	0.01

TABLE 3. (continued)

δRA	δDec	r	cls	m_R	Δm_R	δRA	δDec	r	cls	m_R	Δm_R
QSO 1634+176, z = 1.897, seeing=1.7 arcsec, magnitude limit=22.15											
-23.4	0.7	23.4	g	21.07	0.08	3.4	19.3	19.6	fs	21.29	0.09
-11.0	27.9	30.0	s	18.84	0.01	9.0	10.5	13.8	fs	21.90	0.19
0.0	0.0	0.0	s	18.46	0.01	11.5	0.9	11.5	s	14.76	0.00
0.6	14.6	14.6	fs	21.66	0.13	20.5	20.9	29.3	s	18.11	0.01
2.1	0.4	2.2	fg	20.81	0.20						
QSO 1634+706, z = 1.334, seeing=1.9 arcsec, magnitude limit=21.66											
-17.0	16.5	23.7	fg	20.89	0.10	0.3	28.5	28.5	s	17.32	0.01
0.0	0.0	0.0	s	13.68	0.00						
QSO 1641+399, z = 0.595, seeing=1.7 arcsec, magnitude limit=22.05											
-20.7	10.7	23.3	fs	21.42	0.10	0.0	0.0	0.0	s	17.33	0.00
-16.4	-15.6	22.7	g	21.42	0.10	6.4	-0.9	6.5	fg	21.47	0.11
-11.1	27.8	29.9	fg	21.72	0.13	17.3	6.2	18.3	s	19.75	0.02
QSO 1704+608, z = 0.371, seeing=2.6 arcsec, magnitude limit=21.05											
-2.6	15.6	15.8	s	18.74	0.03	8.8	-26.6	28.0	g	20.11	0.08
-0.7	6.6	6.7	fg	20.44	0.13	25.0	15.5	29.4	fg	20.87	0.16
0.0	0.0	0.0	s	14.83	0.00						
QSO 1715+535, z = 1.929, seeing=1.7 arcsec, magnitude limit=21.80											
-22.8	16.8	28.3	g	20.69	0.07	8.4	0.5	8.4	fg	21.58	0.19
-20.0	-20.1	28.4	fg	21.33	0.12	12.8	24.9	28.0	s	17.84	0.01
0.0	0.0	0.0	s	15.30	0.00	19.7	-1.5	19.8	g	19.70	0.03
2.9	0.6	3.0	s	15.40	0.00						
QSO 1756+237, z = 1.721, seeing=2.7 arcsec, magnitude limit=21.18											
-19.8	11.4	22.8	g	20.85	0.15	0.0	0.0	0.0	s	16.30	0.00
-6.5	26.7	27.5	s	20.68	0.14	7.2	-1.5	7.3	s	18.22	0.01
-6.1	9.1	11.0	s	17.08	0.01	11.4	24.3	26.9	s	19.28	0.04
-3.6	-2.2	4.2	fg	19.62	0.03	12.9	1.6	13.0	g	19.43	0.04
-1.1	4.4	4.5	s	17.31	0.01	22.2	-10.4	24.5	s	18.08	0.01
-0.4	-25.8	25.8	g	20.83	0.14						
QSO 1828+487, z = 0.692, seeing=2.9 arcsec, magnitude limit=21.96											
-23.3	-17.7	29.2	g	20.74	0.07	0.0	0.0	0.0	s	16.59	0.00
-5.6	-7.3	9.2	g	20.08	0.04	26.3	-1.9	26.4	s	16.56	0.00
QSO 2120+168, z = 1.805, seeing=2.2 arcsec, magnitude limit=21.57											
-26.1	6.8	27.0	fg	20.74	0.09	-5.0	-15.2	16.0	s	18.91	0.02
-24.2	4.4	24.6	s	18.89	0.02	0.0	0.0	0.0	s	17.40	0.00
-14.2	-4.8	14.9	s	19.44	0.03	8.0	0.9	8.0	fg	21.47	0.17
-10.1	-0.9	10.1	s	18.03	0.01						
QSO 2145+067, z = 0.990, seeing=3.0 arcsec, magnitude limit=20.93											
0.0	0.0	0.0	s	15.40	0.00						
QSO 2230+114, z = 1.037, seeing=2.1 arcsec, magnitude limit=22.65											
-26.5	14.1	30.0	g	21.60	0.07	13.2	25.1	28.3	s	19.78	0.01
-13.5	5.9	14.7	fg	22.32	0.14	29.2	5.4	29.7	fs	22.20	0.13
0.0	0.0	0.0	s	16.63	0.00						

Notes to TABLE 3

All objects detected above the magnitude limit and within 30 arcsec of each quasar are listed. The columns are δRA, δDec: position offsets measured in arcsec from the quasar, r: distance from the quasar in arcsec, cls: classification (f: faint, g: galaxy, s: star), m_R: apparent R magnitude, Δm_R: formal photometry error in the magnitude.

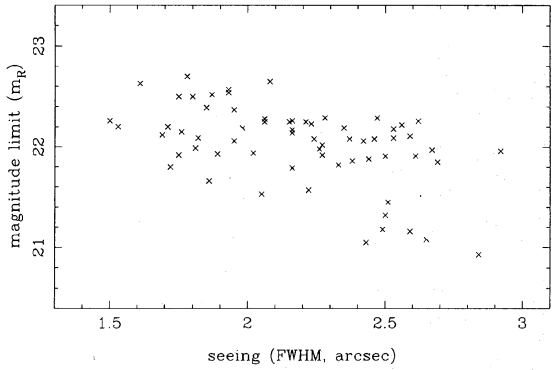

FIG. 1. Estimated magnitude limits as a function of seeing, calculated as described in the text. The data from six nonphotometric fields are not shown.

dius of $r_1=2.0\rho$, slightly larger than optimal to allow for the fact that we have some extended objects. The photometry calculated in this way was converted empirically to values corresponding to fixed apertures of 5 arcsec radius for calibration with the data of Christian *et al.* (1985).

The procedure to estimate the magnitude limit of the FOCAS catalog of a given frame is as follows. First the magnitudes of all the objects are measured with the aperture photometry package using the $r_1=2.0\rho$ radius apertures. The package calculates an error estimate for each measurement based on the aperture size and the variance of the sky background counts. This is not the same as the true error for each galaxy magnitude which we estimate to be twice as large for faint galaxies. The list of magnitudes is then searched for the faintest object for which the error estimate is less than 0.2 mag and the magnitude of this object is adopted as the magnitude limit. The 0.2 mag threshold is arbitrary and nominally indicates that the image has been measured with a SNR of 5. Visual inspection of the data showed that this gave reasonable results, as does the graph of magnitude limit against seeing in Fig. 1. (The data with poor photometry are not included in the figure.) For seeing of FWHM$\leqslant$2.4 arcsec our magnitude limit is $m_R\approx 22$.

3.3 PSF Fitting and Subtraction

The PSF fitting and removal was done using the DAOPHOT package. The standard procedure was used with certain modifications due to the nature of our data. The first step was the creation of a list of bright, unsaturated, and unresolved stars in each frame. Because the quasars were generally bright the list was limited to magnitudes $m_R\leqslant 19$, giving about ten objects per frame. From this list a control star was selected that was closest in magnitude to the quasar and at least 15 arcsec from both the quasar and the edges of the image. A mean PSF for the image was generated from the objects in the bright star list, excluding the quasar. In a few cases (e.g., when the quasar was the brightest object in the field) a satisfactory PSF could not be estimated so no subtraction was possible. These images are noted in Table 1 by the flag "e". Once calculated, the mean PSF was then fitted (by adjusting its amplitude and position) to each of the bright stellar images, and the fitted PSF subtracted from the image out to a radius of ≈ 3 times the seeing FWHM. The results for stellar images other than the quasar were checked in each case to ensure that no artificial structure was introduced by the process; the residual at the location of the quasar was then inspected for new images revealed after the subtraction. The magnitudes of any new images revealed by the subtraction process within about 6 arcsec of the quasar were calculated as above. This radius allowed an overlap with the objects measured by FOCAS so the values could be tested for consistency. Any new objects were then included in the FOCAS catalogues. In the whole sample of 71 quasar images, a total of 4 close galaxies and 3 close stars were added to the catalogues from this analysis.

3.4 Comments on Individual Fields

Some objects in our sample have been imaged previously; these are discussed briefly below, especially with reference to any differences in the faint galaxies detected. We concentrate on objects within 15 arcsec of the quasars. Evidence for variability in the quasar magnitudes is noted in some cases. To facilitate comparisons, we note that $(r-R)_{\rm gal}\sim 0.55$ and $(r-R)_{\rm qso}\sim 0.48$ (Kent 1985).

(1) 0738+313: Hutchings & Neff (1990) found a galaxy 2 arcsec from this quasar. Our DAOPHOT subtracted image reveals a faint galaxy at a separation of 2.6 arcsec.

(2) 0742+318: Imaged by Hutchings & Neff (1990), who found a faint object, $\delta\theta=5.6$ arcsec in seeing of 1.1 arcsec. Yee *et al.* (1986; hereafter referred to as YGS), in poorer seeing, did not see the faint object. In the present work the faint companion is detected at 5.0 arcsec, and the remaining objects in the FOCAS catalogue correspond closely with the results of YGS to a magnitude limit of $m_R\approx 23$, although our catalogue contains about 10% more objects classified as "stars." This implies that our classification of faint objects is slightly more conservative in that we classify fewer doubtful objects as galaxies.

(3) 0952+179: BB91 found no galaxy at the redshift of the Mg II absorption. No close galaxy was found in the present data, although Hutchings (1990) reports that the quasar appears to be extended in a frame taken in 1 arcsec seeing.

(4) 0957+561: This gravitationally lensed double (6 arcsec) image has been extensively studied. Young *et al.* (1980) detected the lensing galaxy 0.8 arcsec from quasar image "B" with $m_r=18.5$. In our DAOPHOT subtracted image we detect this galaxy with $m_R=18.7$ and a larger separation of ≈ 2 arcsec.

(5) 1038+064: BB91 describe an emission-line galaxy with $z=0.441$, $\delta\theta=9.4$ arcsec and $m_r=21.2$. This same galaxy was detected in the present work with $m_R=20.8$.

(6) 1049+616: YGS found three nearby galaxies: 1: $\delta\theta=3.7$ arcsec, $m_r=20.88$, 2: $\delta\theta=13.5$ arcsec, $m_r=22.83$, 3: $\delta\theta=14.2$ arcsec, $m_r=22.57$. Only the first was detected in the present work with $\delta\theta=2.9$ arcsec $m_R=19.1$, since the poor seeing (2.7 arcsec) gave a bright ($m_R<21.9$)

magnitude limit for the frame. The value we obtain for the galaxy magnitude is quite uncertain because of the difficulty in doing the subtraction.

(7) 1103−006: YGS found three close galaxies: 1: $\delta\theta=17$ arcsec, $m_r=19.44$, 2: $\delta\theta=11$ arcsec, $m_r=22.82$, 3: $\delta\theta=13$ arcsec, $m_r=22.11$. Our data, taken in seeing of 2.3 arcsec had a magnitude limit of $m_R<21.9$ and only detected the first with $m_R=19.64$.

(8) 1104+167: YGS found the following close galaxies: 1: $\delta\theta=14$ arcsec, $m_r=22.39$, 2: $\delta\theta=17$ arcsec, $m_r=20.22$, 3: $\delta\theta=15$ arcsec, $m_r=20.96$. All of these were detected in the present work in seeing of 1.7 arcsec with $m_R=21.8$, 20.8, 21.0, respectively.

(9) 1115+080: This quasar is gravitationally lensed with multiple images. Christian *et al.* (1987) describe the four components of the quasar image as well as the detection of the lensing galaxy at a distance of 1.4 arcsec from quasar component "C" with $m_R=20.2$. Our DAOPHOT analysis reveals the quasar components "A" and "C" but, although additional components remained they could not be separated reliably.

(10) 1127−145: BB91 found an emission-line galaxy at $z=0.313$, $\delta\theta=9.6$ arcsec, $m_r=19.3$ and another companion at $\delta\theta=5.3$ arcsec, $m_r=22.4$. The first was detected in the present work with $\delta\theta=9.4$ arcsec, $m_R=20.1$. The second was fainter than our limit of $m_R<21.3$.

(11) 1209+107: Cristiani (1987) in seeing of 1.4 arcsec has found a galaxy at $z=0.3922$, $\delta\theta=7.1$ arcsec, and $m_r=21.9$. Hutchings (1990) describes a close ($\delta\theta\approx1$ arcsec) galaxy with $m_R=19.5$. Arnaud *et al.* (1988) in seeing of 0.8 arcsec find two galaxies: 1: $\delta\theta=1.3$ arcsec, $m_R=22.3\pm0.6$,2: $\delta\theta=7$ arcsec, $m_R=21.3$. Both these were detected in the present work, with magnitudes of $m_R=22.7$ and 21.6, respectively, although only the second was included in our final catalogue with a magnitude limit of $m_R<22.3$.

(12) 1332+552: Miller *et al.* (1987) found an absorption line galaxy at $z=0.373$, $\delta\theta=5.0$ arcsec and BB91 give $m_V=20.7$. This was found here at $\delta\theta=5.5$ arcsec, $m_R=19.6$ along with a fainter galaxy at $\delta\theta=7$ arcsec.

(13) 1354+594: Ellingson *et al.* (1991) found two galaxies at $\delta\theta=8$ arcsec with $m_r=21.91$,21.46. These were also found in the present work, with $m_R=21.7$, 21.4.

(14) 1511+103: Bergeron (1988) found an emission line galaxy at $z=0.437$, $\delta\theta=6.7$ arcsec and $m_r=22.0$. This was not detected in the present work, with a magnitude limit of $m_R<21.1$.

(15) 1512+370: Hickson & Hutchings (1987) found a galaxy at a separation of $\delta\theta\approx10$ arcsec with redshift $z=0.370$ as well as some structure extending East from the quasar. We detect this galaxy with $\delta\theta=10.5$ arcsec, $m_R=19.9$, and also note that the quasar is extended to the East.

(16) 1641+399: YGS found three galaxies: 1: $\delta\theta=6.8$ arcsec, $m_r=20.78$; 2: $\delta\theta=5.1$ arcsec, $m_r=22.6$; 3: $\delta\theta=10.2$ arcsec, $m_r=22.5$ and for the quasar magnitude they found $m_r=15.47$. The brightest of these galaxies was detected ($m_R=21.5$) in the present work in 1.7 arcsec seeing, but the other two were fainter than the magnitude limit of $m_R<22.1$. We measured the quasar magnitude as $m_R=17.33$, almost 2 mag fainter than the value of YGS. This was confirmed by relative photometry with other objects in the field; this quasar is known to exhibit large optical variations (see Bregman *et al.* 1986).

(17) 1704+608: Hutchings & Neff (1990) found a galaxy at $\delta\theta\approx7.5$ arcsec which corresponds to our detection of a $\delta\theta=6.8$ arcsec, $m_R=20.4$ galaxy.

(18) 1828+487: YGS found close galaxies at $\delta\theta=8$ arcsec, $m_r=22.71$, and $\delta\theta=12$ arcsec, $m_r=22.82$. These were not detected in our rather poor data with seeing of 2.9 arcsec and a magnitude limit of $m_R<22.0$. We note a change in the quasar magnitude, measuring $m_R=16.59$ compared to $m_r=17.50$ by YGS.

(19) 2145+067: Bergeron (1988) found an emission-line galaxy at $z=0.790$, $\delta\theta=5.9$ arcsec, and $m_r=22.1$. This was not detected in the present work due to poor seeing (3.0 arcsec; magnitude limit $m_R<20.9$), though a change in the quasar magnitude is noted. We measure $m_R=15.40$ compared to $m_r=16.45$ by Bergeron.

4. QUASARS WITH DETECTED Mg II ABSORPTION

4.1 Sample

In this section we discuss the properties of the galaxies found close to the quasars in which Mg II absorption has been detected. The redshifts of the detected galaxies are not yet available, so we use a statistical approach to determine which of these galaxies are most likely to be associated with the absorption systems. In order to reduce the probability of detecting even very bright galaxies at the quasar redshift, we limit the sample to quasars at redshifts $z>0.9$. There are 58 quasars in our sample satisfying this criterion. The 17 quasars with lower redshifts are discussed separately in Sec. 6.

With a limiting magnitude for galaxy detection of $m_R\approx22$ we are unlikely to detect any normal galaxies at redshifts above $z=0.7$. We therefore only consider absorption systems detected at redshifts $z_{abs}\leqslant0.7$. 17 of the quasars have known Mg II absorption systems satisfying this criterion. The detection thresholds vary somewhat between the different surveys, but those that quote limits tend to have a cutoff in rest equivalent-width of about 0.6 Å. In summary, the high redshift quasar sample is divided into 17 with Mg II absorption and 41 without absorption.

For the high redshift sample the properties of the images of quasars with and without Mg II absorption were compared. This is in order to show that any statistical detection of galaxies associated with the Mg II absorption is not due to any systematic difference in the properties of the images. The distributions of quasar redshift, quasar apparent magnitude, seeing and limiting magnitude are compared for the two samples in Table 4. The two-sample Kolmogorov–Smirnov test shows that the quasar redshifts, magnitudes, and the seeing do not differ significantly between the two samples. There is, however, a small but significant difference in limiting magnitude between the two samples. The Mg II sample has a mean limiting magnitude 0.3 mag brighter than the sample in which Mg II

TABLE 4. Properties of Mg II and non-Mg II images.

	Mg II		non-Mg II			
property	mean	rms	mean	rms	D	P_{KS}
z_{qso}	1.638	0.358	1.694	0.324	0.231	0.54
$m_{R,qso}$	16.48	0.97	17.05	0.71	0.360	0.09
seeing(")	2.11	0.37	2.18	0.31	0.301	0.20
$m_{R,lim}$	21.82	0.46	22.13	0.31	0.400	0.05

Notes to TABLE 4

D is the test statistic from the 2-sample Kolmogorov-Smirnov test. P_{KS} is the significance level for the null hypothesis that the samples are drawn from the same distribution.

was not detected. This is because we preferentially observed quasars from the Mg II sample in the earlier observing sessions, some of them in poorer conditions. This trend will only bias against the detection of faint galaxies near the quasars which show absorption compared to those quasars which show no absorption.

4.2 Detection of Galaxies and Absorption Systems

In the previous section we have shown that the images of the Mg II quasars have no properties that will make the detection of close galaxies more likely than in the images of the non-Mg II quasars. We can therefore use a statistical approach to identify galaxies likely to be associated with the absorption systems. This is done by finding any galaxies significantly closer to the line-of-sight to a quasar than we might expect by random chance. The significance is estimated using the nearest-neighbor test because the absorber is likely to be the closest object and this test is not distorted as much by the effects of galaxy clustering as other tests such as the correlation function.

Under a random distribution the distance to the nearest neighbor of each quasar will be distributed as a Poisson distribution, a function of the mean surface density of galaxies in each field. Since this mean surface density varies between fields, we normalize by this density to define a statistic

$$S=1-e^{-\pi\rho r^2},$$

where ρ is the mean surface density of galaxies in a given field and r is the distance from the quasar to the nearest galaxy in that field. For the random or Poisson case (no quasar–galaxy correlation), the statistic S then has a uniform distribution in the range (0 to 1) which is independent of variations in surface density and magnitude limit from field to field.

We would expect the mean value of S to be 0.5 for randomly distributed galaxies, and calculation of the statistic for galaxies counted near the control stars in all 58 fields does indeed give a mean value of S of 0.51. The mean values of S for galaxies counted near the quasars in the Mg II and the non-Mg II samples however are 0.22 and 0.41, respectively. The Kolmogorov–Smirnov test gives probabilities of 0.1% and 5%, respectively, that these are drawn from uniform random distributions. The fact that both these samples are significantly different from the random case implies that low redshift galaxies are clustered close to the line of sight to bright high redshift quasars, independent of the detection of Mg II absorption. This interesting result is discussed further in Paper II. The important point here is the difference between the two distributions. The two-sample Kolmogorov–Smirnov test gives an 7% probability of these samples being drawn from the same distribution. The nearest-neighbors to the Mg II quasars are therefore significantly closer than the neighbors of the non-Mg II quasars so we infer that there is statistical evidence that we are detecting galaxies associated with the absorption systems.

The value of the S statistic can be used to indicate in which of the 17 Mg II quasar fields we are most likely to have detected a galaxy associated with the absorption system. The values of S for each field are shown in Table 5 as well as the (absolute) luminosities and impact parameters of the galaxies under the hypotheses that they are situated at the absorption redshift. These parameters are calculated for the nearest-neighbor galaxy to each quasar as well as any other galaxies within 15 arcsec of the quasar. Details of the calculation of luminosity and luminosity function are given in the Appendix. Note that some of the quasars have two absorption systems; in this case the calculations are repeated in the table for both systems. However, for the purposes of compiling statistics of the detected galaxies below, the values for the lower absorption redshift are used. The table also gives the luminosity at the absorption redshift equivalent to the apparent magnitude limit of each CCD image. This provides a useful indication in some cases that the data are not good enough to have detected an absorbing galaxy—either because of poor data or because the absorption redshift is too high.

(1) There are 10 quasars for which the nearest galaxy statistic $S\leqslant 0.2$ (i.e., for each quasar, the probability that they would be found as close as this is $<20\%$ in a random distribution). The corresponding galaxies all have impact parameters of $b<30h^{-1}$ kpc and their luminosities lie in the range $0.1<L/L_*<1.3$. These we tentatively identify with the absorbers and label "A" in Table 5. We note that this is only a statistical identification and that some of the close galaxies may not be associated with the absorption.

(2) There are two doubtful fields (0952+179 and 0958 +551) with reasonable magnitude limits but with more distant galaxies ($S\approx 0.3$, $b\approx 50h^{-1}$ kpc). These have plausible luminosities to be at the absorption redshift, but are too far from the line of sight to the quasars to be identified unambiguously with the absorbers without redshift information and are labeled "?" in the table. It will be interesting to obtain the redshifts of these galaxies.

(3) Four frames have no close galaxies detected (0843 +136, 0848+163, 1246−057, and 1511+103). In each case the nearest detected galaxy has a luminosity $L>2L_*$ and impact parameter $b>60h^{-1}$ kpc, not consistent with normal galaxies at the absorption redshift, although we cannot discount the possibility that these are giant elliptical galaxies in groups associated with the absorption systems. We denote these as nondetections labeled "m" (for "miss") in the table. Cases where galaxies producing the absorption system have not been detected are interesting

TABLE 5. Statistics of galaxies near quasars with Mg II absorption.

QSO (1)	z_1 (2)	z_2 (3)	z_{abs} (4)	m_{gal} (5)	r (6)	S (7)	p_z (8)	b_{z1} (9)	b_{z2} (10)	l_{mab} (11)	l_{abs} (12)	b_{abs} (13)	Abs (14)
0843+136	0.18	0.69	0.605	20.2	16.0	0.32	0.78	31.3	63.6	0.5	2.6	61.1	m
0843+136	0.18	0.69	0.607	20.2	16.0	0.32	0.78	31.3	63.6	0.5	2.6	61.2	"
0848+163	0.27	0.72	0.586	19.6	16.3	0.31	0.45	42.1	65.6	0.4	3.9	61.7	m
0848+163	0.27	0.72	0.590	19.6	16.3	0.31	0.45	42.1	65.6	0.4	4.0	61.8	"
0952+179	0.14	0.80	0.238	20.9	23.0	0.33	0.92	37.2	94.5	0.1	0.1	54.6	?
0958+551	0.18	0.65	0.241	21.9	17.7	0.35	0.69	34.7	69.3	0.0	0.1	42.6	?
1038+064	0.18	0.80	0.442	20.6	7.3	0.06	0.83	14.3	30.1	0.3	0.8	24.7	A
1038+064	0.18	0.80	0.442	20.8	9.7	0.10	0.84	19.0	40.0	0.3	0.6	32.8	"
1127−145	0.17	0.42	0.313	20.1	9.4	0.12	0.61	17.7	31.0	0.2	0.6	26.5	A
1148+387	0.11	0.80	0.213	21.0	3.3	0.03	0.94	4.4	13.6	0.0	0.1	7.3	A
1148+387	0.11	0.80	0.553	21.0	3.3	0.03	0.94	4.4	13.6	0.2	0.9	12.3	"
1209+107	0.29	0.80	0.393	21.6	7.1	0.09	0.71	19.2	29.4	0.1	0.2	22.8	A
1209+107	0.29	0.80	0.629	21.6	7.1	0.09	0.71	19.2	29.4	0.4	0.8	27.6	"
1246−057	0.43	0.80	0.640	20.7	41.5	0.97	0.32	138.4	170.9	0.5	2.0	161.5	m
1317+277	0.22	0.80	0.289	21.9	7.8	0.05	0.79	17.7	32.3	0.1	0.1	21.1	A
1317+277	0.22	0.80	0.660	21.9	7.8	0.05	0.79	17.7	32.3	0.7	0.7	30.8	"
1329+412	0.34	0.76	0.501	22.1	2.4	0.01	0.57	7.2	9.9	0.3	0.3	8.7	A
1332+552	0.22	0.53	0.374	19.8	5.5	0.02	0.59	12.3	19.9	0.3	1.1	17.0	A
1332+552	0.22	0.53	0.374	21.1	7.3	0.03	0.56	16.6	26.7	0.3	0.3	22.8	"
1421+330	0.24	0.69	0.457	21.8	6.4	0.04	0.70	15.4	25.5	0.2	0.3	22.0	A
1511+103	0.18	0.53	0.437	19.5	23.4	0.43	0.67	45.7	85.1	0.5	2.0	78.4	m
1634+706	0.22	0.80	0.669	20.9	23.7	0.51	0.78	53.4	97.4	0.9	1.9	93.3	−
1715+535	0.34	0.76	0.367	21.6	8.4	0.17	0.58	24.9	34.3	0.2	0.2	25.9	A
1756+237	0.16	0.62	0.371	19.6	4.2	0.02	0.79	7.6	16.2	0.3	1.2	13.1	A
1756+237	0.16	0.62	0.371	19.4	13.0	0.20	0.77	23.3	50.1	0.3	1.5	40.3	"

Notes to TABLE 5

1: quasar name, 2,3: the redshift range searched for Mg II absorption, 4: absorption redshift, 5: apparent R magnitude of galaxy, 6: distance between galaxy and quasar in arcsec, 7: S statistic, 8: probability that the galaxy redshift is in $[z_1,z_2]$, 9,10: the impact parameters of the galaxy if at z_1,z_2 (h^{-1}kpc), 11: the limiting luminosity at z_{abs} corresponding to the apparent magnitude limit of the frame (L/L_*), 12,13: the luminosity (L/L_*) and impact parameter (h^{-1}kpc) of the galaxy if at z_{abs}, 14: detection flag (A: absorber detected, ?: ambiguous identification, m: no absorber detected, −: poor data).

and are discussed further in Sec. *4.4* below. However, the detection limits in each of these cases correspond to $0.5L_*$ so it is possible that the data are not sensitive enough to detect the absorber galaxies (see below).

(4) Finally, there is one quasar (1634+706) in which no close galaxies are detected due to poor data; the luminosity limit at the absorption redshift is $\approx L_*$ making detection unlikely. This is designated "-" in the table.

In summary, we discard one frame because of poor data; of the 16 remaining there are ten probable detections, two doubtful and four probable nondetections.

Five of the above quasars are listed by BB91 with galaxies detected at the absorption redshift: 1038+064, 1127−145, 1209+107, 1332+552, and 1511+103. In the case of 1511+103, the galaxy they detected was fainter than our magnitude limit. In all the other cases we independently detect the galaxy and identify it as the absorber. This correspondence supports our association of the nearest-neighbor galaxies with the absorption systems.

4.3 Properties of the Close Galaxies

The ten galaxies we denote as being probably associated with Mg II absorption have luminosities $0.1 < L/L_* < 1.3$ and a mean luminosity of $\langle L/L_* \rangle = 0.5$ (assuming they are at the absorption redshift in each case). This corresponds to an absolute R magnitude of $M_R = -20.0$ ($H_0 = 100$ km s^{-1} Mpc^{-1}, and intermediate galaxy type). In agreement with Bechtold & Ellingson (1992) we find no evidence for a deficiency of absorber galaxies with $L/L_* < 0.3$ as reported by BB91. We do note that our assumption that the nearest-neighbor galaxy is associated with the absorption system at lower redshift when there is more than one system will bias our luminosity estimates to lower values. However this only affects the quasars 1148+387 and 1317+277; if we locate the galaxies in these two cases at the higher absorption redshift the mean luminosity is still only $\langle L/L_* \rangle = 0.6$.

We also considered the distribution of rest equivalent width of the absorbers as a function of impact parameter.

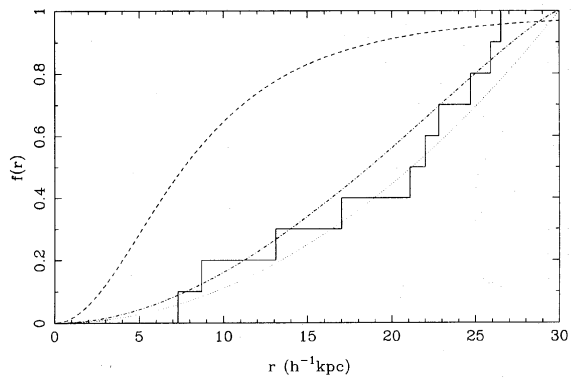

FIG. 2. Cumulative frequency distribution of the impact parameters of the galaxies detected and identified as Mg II absorbers close to the lines of sight to ten quasars (solid histogram). The curves show the distributions predicted for three models: a uniform distribution (dots), a randomly inclined disk (dash–dot) and a centrally-condensed distribution (dashes).

The data for two of the quasars came from samples with poorly defined detection limits and were discarded. The remaining eight systems all had rest equivalent widths in the range $0 < W_{\rm rest} < 1$ Å. There is no obvious trend in this distribution; the Spearman Rank coefficient $r_S = 0.33$ indicating no significant correlation.

It is interesting to consider the possibility that the galaxies we detect are in clusters or groups. To do this we calculated the S statistics centered on the nearest-neighbor galaxy to each quasar, to determine if the other galaxies were clustered around that one. The mean value of S found was 0.50 and the Kolmogorov–Smirnov probability that the sample was drawn from a uniform random distribution was 87%. Similar results were obtained for the non-Mg II sample. Thus we do not find any evidence for clustering around the absorber galaxies, although it should be noted that the typical scales considered here are of the order $100h^{-1}$ kpc, whereas the scale length of the galaxy correlation function is of the order of $4h^{-1}$ Mpc.

The mean impact parameter of the ten detected galaxies is $\langle r \rangle = 19h^{-1}$ kpc. However, we do note that any galaxies further than $40h^{-1}$ kpc from the line of sight were rejected. This limit is based on the arbitrary statistical limit of $S < 0.2$, but is reasonable because the distribution of all 17 impact parameters has a clear break at about $30h^{-1}$ kpc. This is similar to the results of BB91 who quote $\langle D/R_H \rangle = 2.3$ or $\langle D \rangle = 25h^{-1}$ kpc using their relation $R_H = 22h_{50}^{-1}$ kpc. The actual distribution of impact parameters tell us more than the mean value. Figure 2 shows the integral distribution of impact parameters of the galaxies assuming they are at the absorption redshift. We compare this distribution with that predicted for three simple models of the absorbing systems, ranging from a constant absorber density to that of a centrally-condensed distribution. These are also shown in the figure; the models are normalized to unity at a radius of $30h^{-1}$ kpc.

To calculate the models we assume galaxies are sparsely distributed so that only one enters the problem for each quasar. We further assume a distribution function of absorbing clouds about each galaxy of $p(r)$ such that a line of sight passing within a distance r of the galaxy center has a probability p of being absorbed by an Mg II cloud of the appropriate column density. We must also consider the effect of any bias due to gravitational lensing of the quasars on the statistics; we consider separately the cases of lensed and nonlensed quasars.

(i) Nonlensed. The actual distribution of the separations of the quasar and the galaxy center is $a(r)dr \propto r\,dr$. We only include those that give rise to absorption and so the observed distribution is $o(r)dr \propto p(r)a(r)dr$. The probability distribution of separations in the sample is

$$f(<r) = \frac{\int_0^r r' p(r') dr'}{\int_0^\infty r' p(r') dr'}.$$

(ii) Lensed. The quasars are only in the sample because they are lensed. If the surface density of lenses is $\Sigma_l(r)$ then the probability that at a particular radius the quasar will be both lensed and absorbed is $p(r)\Sigma_l(r)$. Hence

$$f_l(<r) = \frac{\int_0^r r' p \Sigma_l\, dr'}{\int_0^\infty r' p \Sigma_l\, dr'}.$$

Note that as Σ_l is centrally condensed (typically $\propto r^{-1}$) this will bias the distribution to smaller separations.

We now calculate the distributions for three models.

(1) A spherically-symmetric cloud distribution giving a centrally-condensed distribution of surface density. In practice, we do not know the form of the distribution, so we choose a simple functional form for p which can be integrated, namely

$$p(r) = \left[1 + \left(\frac{r}{a}\right)^2\right]^{-s/2},$$

with $0 < r < R$. This is easily integrated to give f (it converges for $s > 2$). In the case of gravitational lensing, the corresponding integral is difficult so for that case we use

$$p(r) = \left[1 + \left(\frac{r}{a}\right)\right]^{-s},$$

which is an equally valid functional guess and the integral converges for $s > 1$. Both of the above can also be used with an outer cutoff, but the core radius a and the power s are more realistically constrained if there is no cutoff to the integrals. The constraint we use is $f(r < R) \geqslant 0.95$ for the maximum radius R. One such distribution is shown in Fig. 2 for $a = 10h^{-1}$ kpc, $s = 5$. This is clearly much more centrally condensed than the data, as are any realistic models with core radii similar to the luminous portions of galaxies.

(2) A uniform disk of radius R, averaged over all inclinations, θ, the angle between the normal to the disk and the line of sight. The position of the absorber is defined by polar coordinates (r,ϕ) in the plane perpendicular to the line of sight. We have

$$p(r,\theta,\phi) = \begin{cases} 1 & r < R\cos\theta \\ 1 & r > R\cos\theta \text{ and } r^2(\cos^2\phi + \sin^2\phi/\cos^2\theta) < R^2 \\ 0 & r > R\cos\theta \text{ and } r^2(\cos^2\phi + \sin^2\phi/\cos^2\theta) > R^2. \end{cases}$$

Now we average over θ and ϕ. Averaging over ϕ for fixed r and θ gives

$$\langle p(r,\theta)\rangle = \begin{cases} 1 & r < R\cos\theta \\ \dfrac{2\phi}{\pi} & r > R\cos\theta, \end{cases}$$

where ϕ is the solution of $r^2(\cos^2\phi + \sin^2\phi/\cos^2\theta) = R^2$. Averaging next over $\mu = \cos\theta$,

$$\langle p(r)\rangle = 1 - \frac{r}{R} + \frac{2}{\pi}\int_0^{r/R} \phi\, d\mu,$$

where

$$\cos^2\phi = \frac{1-(R/r)^2\mu^2}{1-\mu^2}.$$

The resulting expression must still be integrated over radius to give $f(<r)$. We do this numerically to give the second function plotted in Fig. 2. This is much closer to the observed distribution than the first case; the Kolmogorov–Smirnov test gives a probability of 75% (nonlensed) that the data are consistent with this distribution. However, any realistic disk model would include a decreasing density with radius, making this more condensed and less like the data.

(3) A uniform distribution with, necessarily, a sharp (observational) cutoff at a maximum radius R, so

$$p(r) = \begin{cases} 1 & r < R \\ 0 & r > R \end{cases}$$

which is easy to integrate for the distribution function with and without lensing:

$$f = \left(\frac{r}{R}\right)^2,$$

$$f_l = \left(\frac{r}{R}\right).$$

This is the most extended distribution modeled and is close to the observed data. The Kolmogorov–Smirnov gives a probability of 72% (nonlensed) that the data are consistent with this distribution.

The same three models are replotted in Fig. 3 for the case where the statistics are biased by gravitational lensing. This biases the distributions to small separations to the extent that all of the models can be rejected at Kolmogorov–Smirnov confidence levels of 70% or more. This suggests that the effect of gravitational lensing is not significant in this sample, although it could be hidden if our data were very incomplete at small separations. It is also possible that the gravitational lens distribution is not centered on the nearest-neighbor galaxies.

In the absence of any significant lensing bias, our data are best represented by the models in which the galaxies are drawn from uniform distributions at least about $30h^{-1}$ kpc in radius. The actual distribution will probably extend beyond $30h^{-1}$ kpc. It is possible that the absorbing cloud and the observed galaxy are both components of a larger dynamical system although we do not find evidence for

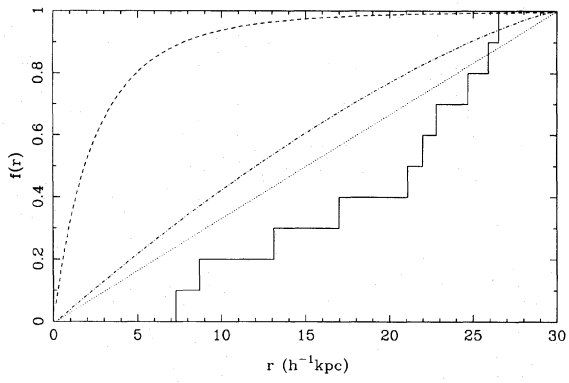

FIG. 3. Cumulative frequency distribution of the impact parameters of the galaxies detected and identified as Mg II absorbers close to the lines of sight to ten quasars (solid histogram). The curves show the predictions of the three models described in the previous figure with the additional effect of gravitational lensing.

groups of galaxies. The velocity data reviewed in the introduction shows that some Mg II systems have a velocity spread of over 600 km s^{-1} which implies the systems may be larger than single galaxy halos.

4.4 Mg II QSOs with No Close Galaxies

It would be very interesting if we could demonstrate a case of Mg II absorption for which there was no corresponding galaxy detected. There are four cases listed above where no galaxy was detected. In each case, however, the limiting luminosity was about $0.5L_*$ and, since some of the confirmed absorbers have luminosities as low as $0.2L_*$, the absorbers may be below the detection limits in these cases. This can be quantified as follows: we can predict the number of absorbers that should have been detected in the sample, given the magnitude limits achieved. We assume that every one of the Mg II quasars has an absorber galaxy and that these galaxies are drawn from the standard luminosity function weighted by luminosity. For each quasar we have already found the luminosity at the absorption redshift that corresponds to the apparent magnitude limit.

The probability of detection is then given by the fraction of all galaxies brighter than this limit in the luminosity-weighted distribution function. The sum of these probabilities is the expected number of galaxies detected. This was calculated for the 17 quasars in Table 5. The sum of the probabilities is 11.2. With ten galaxies detected, it is apparent that there is no evidence in our sample for absorption without a close galaxy being present. Even if some of the "probable" detections arose by chance (see Sec. *4.2*), the difference is unlikely to be significant.

There is a further reason why we would not expect to see galaxies in all cases: if the galaxy is *too close* to the line of sight to the quasar, it will be confused with the seeing disk of the quasar and at the closest separations, undetectable even with DAOPHOT. We can estimate the number of galaxies affected: for $R \leqslant 30h^{-1}$ kpc, $\theta \leqslant 8$–15 arcsec, and for a mean separation of $\theta = 10$ arcsec the total area is 314 square arcsec. If the quasar seeing disk area ≈ 12 square

arcsec we have 1/25 of the total area hidden and would expect to miss one object in the sample.

We can now address the first question of this study: are all Mg II systems associated with a close galaxy? The data are consistent with this interpretation, but we note the possibility that the absorbers are part of larger mass concentrations.

5. QUASARS WITH NO DETECTED Mg II ABSORPTION

The 38 high redshift quasars with no detected Mg II absorption are listed in Table 6. This sample also shows an excess of close galaxies. It is therefore interesting to consider the possibility that these lie in the redshift range searched but are not producing any absorption.

To do this we consider a very simple model in which the absorbers consist of extended distributions with a constant covering factor f out to a maximum radius Rh^{-1} kpc. For a given galaxy, we would therefore expect to see absorption (with a probability f) if the galaxy lies within Rh^{-1} kpc of the line of sight to the quasar and its redshift is in the observed range [z1,z2]. Since the galaxy redshifts are not available, we estimate the probability that the detected galaxy at its measured apparent magnitude, lies within the redshift range, assuming it is drawn at random from the luminosity function. For a model with a given value of R, the probability that a galaxy causes absorption is given by

$$p(R)=\begin{cases}0, & R<bz_1\\ fp_z[m_g,z_1,\min(z_2,z_R)], & bz_1\leqslant R,\end{cases}$$

where $[z_1,z_2]$ is the redshift range searched for Mg II absorption, bz_1 is the impact parameter the galaxy would have at a redshift of z_1, and z_R is the redshift at which the galaxy would have an impact parameter of R. As discussed in the Appendix, $p_z(m_g,z_1,z_2)$ is the probability that a galaxy of apparent magnitude m_g drawn from the standard luminosity function has a redshift in the range $[z_1,z_2]$.

To calculate the expected number of detected absorption systems we just sum the above probabilities for all the galaxies near the quasars in our sample. The ratio of this number to the actual number of absorbers detected in the subsample is the covering factor. This is shown plotted as a function of R in Fig. 4. Radii less than $20h^{-1}$ kpc are not shown because of the constraint that at least as many quasars exhibit absorption as in the data. The figure shows that for values of $R\approx 30h^{-1}$ kpc the model is consistent with a covering factor of unity [$f(30)=1.1\pm 0.2$]. At $R=40$ the covering factor is smaller but still consistent with a value of unity. Values of R larger than $50h^{-1}$ kpc would give covering factors significantly smaller than unity, but these would not be consistent with the distribution of observed galaxies discussed in the previous section

Our answer to the second question is therefore that the data are consistent with a model in which all the visible ($m_R\lesssim 22$) galaxies have associated Mg II absorption with a covering factor of unity out to a radius of $30h^{-1}$ kpc. In reality however, we know that we have not detected all the galaxies associated with absorption (e.g., 1511+103; see Sec. *4.2*). Allowing for this incompleteness would give either a smaller covering factor or a smaller maximum radius.

There is evidence for a covering factor less than unity from other observations of galaxies where no absorption is detected. In the double quasar 0957+561, the lensing galaxy is a bright giant elliptical almost directly on the line of sight to one component of the double image, but no absorption is detected (Young *et al.* 1982). More recent observations of galaxies with known redshifts by Bechtold & Ellingson (1992) reveal three galaxies closer than $30h^{-1}$ kpc to quasar lines of sight that did not produce absorption. Bechtold and Ellingson note that the galaxies not causing absorption did not have strong emission lines and had spectra like ellipticals. As we might expect, gas poor elliptical galaxies do not seem to be good absorbers. Previous examples of identified absorber galaxies tend to have strong emission lines (see BB91) consistent with spiral types. If the absorbers are preferentially spiral galaxies, their redshifts should be easy to determine from emission lines. The close galaxies we detect with no associated Mg II absorption are among the most interesting objects to follow up from this study.

6. LOW REDSHIFT QUASARS

The properties of galaxies found near the 13 low-redshift quasars are given in Table 7. These are treated separately because at these low redshifts we cannot exclude the possibility of detecting galaxies at the quasar redshift. Any clustering of galaxies physically associated with the quasar would then distort the nearest-neighbor statistics, invalidating the approach used above to identify possible absorbers. There is some evidence for this from the nearest-neighbor statistics: the mean value of S is 0.26 for this sample compared to 0.35 for the high redshift sample, although the Kolmogorov–Smirnov test shows that the distributions of S are not significantly different for the two samples. We therefore do not find strong evidence of clustering at the quasar redshifts; furthermore, none of the known absorption systems in this sample are at the quasar redshifts. Bechtold & Ellingson (1992) remark that galaxies in clusters associated with the quasars may be less optically thick in absorption than ordinary galaxies because galaxies in dense environments do not contain much cold gas.

There are five quasars in the low redshift sample with known Mg II absorption. Using the same criterion of $S\leqslant 0.2$ as above we tentatively associate the closest galaxy to four of these (0738+313, 1049+616, 1354+195, and 1704+608) with the absorption system. We do not find a galaxy associated with the quasar 0742+318 in agreement with Bechtold & Ellingson (1992) who also confirm that the galaxy we detect close to quasar 1354+195 is at the absorption redshift. If the galaxies we detect here are at the absorption redshifts, their mean properties are $\langle L/L_*\rangle=0.3$ and $\langle r\rangle=12h^{-1}$ kpc, slightly fainter and closer than for the high redshift sample, although the difference is not significant because of the small numbers and the greater uncertainty in the galaxy redshifts.

TABLE 6. Statistics of galaxies near quasars with no Mg II absorption at $z_{abs} < 0.7$.

QSO (1)	z_1 (2)	z_2 (3)	z_{abs} (4)	m_{gal} (5)	r (6)	S (7)	p_z (8)	b_{z1} (9)	b_{z2} (10)	l_{mab} (11)	z_l (12)	b_l (13)
0736−063	0.26	0.80	-	20.4	4.1	0.05	0.66	10.3	16.7	-	0.5	14.0
0736−063	0.26	0.80	-	21.4	8.0	0.17	0.75	20.2	32.9	-	0.6	31.3
0736−063	0.26	0.80	-	20.8	11.6	0.32	0.71	29.1	47.6	-	0.5	42.4
0835+580	0.22	0.55	-	21.6	6.9	0.08	0.56	15.6	25.5	-	0.7	27.4
0835+580	0.22	0.55	-	21.1	9.0	0.13	0.61	20.4	33.4	-	0.6	34.3
0836+195	0.22	0.54	-	22.0	10.4	0.09	0.49	23.5	38.2	-	0.8	42.5
0854+191	0.24	0.68	-	21.5	13.0	0.17	0.71	31.0	51.3	-	0.6	50.6
0856+170	0.18	0.53	-	21.4	10.5	0.11	0.59	20.5	38.1	-	0.6	40.9
0856+189	0.20	0.46	-	20.5	45.4	0.97	0.56	95.8	155.8	-	0.5	158.7
0957+561	0.21	0.38	-	18.7	2.0	0.01	0.36	4.4	6.3	-	0.2	4.8
0957+561	0.21	0.38	-	20.8	11.2	0.32	0.34	24.5	35.1	-	0.5	40.8
0957+561	0.21	0.38	-	20.7	9.2	0.23	0.34	20.2	29.0	-	0.5	33.4
0957+561	0.21	0.38	-	21.4	12.4	0.37	0.28	27.0	38.7	-	0.6	48.0
0957+561	0.21	0.38	-	19.7	7.8	0.17	0.43	17.1	24.6	-	0.4	23.9
1017+280	0.27	0.80	-	20.5	18.3	0.20	0.63	47.1	75.1	-	0.5	63.9
1054−034	0.29	0.80	-	19.8	5.7	0.05	0.46	15.4	23.5	-	0.4	17.6
1055−045	0.17	0.57	-	22.4	35.1	0.83	0.54	65.8	131.2	-	0.8	146.0
1115+080	0.19	0.71	-	20.3	12.4	0.23	0.80	25.3	49.7	-	0.4	42.2
1126+101	0.14	0.52	-	20.5	7.7	0.08	0.77	12.4	27.8	-	0.5	26.9
1126+101	0.14	0.52	-	20.0	9.7	0.13	0.81	15.7	35.1	-	0.4	31.3
1126+101	0.14	0.52	-	20.5	10.3	0.14	0.77	16.7	37.4	-	0.5	36.2
1138+040	0.34	0.76	-	21.2	17.3	0.50	0.56	51.1	70.3	-	0.6	66.2
1148−001	0.23	0.76	-	20.9	29.5	0.53	0.75	68.6	120.0	-	0.5	108.9
1211+334	0.19	0.57	-	21.5	21.9	0.57	0.66	44.6	82.0	-	0.7	85.9
1215+113	0.21	0.53	-	20.9	46.4	0.84	0.60	101.5	169.2	-	0.6	172.7
1225+317	0.29	0.80	-	21.7	8.8	0.05	0.71	23.6	36.1	-	0.7	35.1
1228+078	0.22	0.71	-	20.4	34.3	0.66	0.72	77.5	137.4	-	0.5	117.9
1246+377	0.14	0.80	-	19.3	67.7	0.91	0.81	109.6	278.7	-	0.3	189.9
1256+357	0.24	0.67	-	22.0	7.8	0.09	0.65	18.6	30.6	-	0.8	31.7
1257+346	0.14	0.80	-	21.7	32.7	0.81	0.90	52.8	134.4	-	0.7	130.2
1258+286	0.24	0.71	-	21.1	24.9	0.34	0.74	59.7	99.9	-	0.6	94.5
1303+308	0.29	0.53	-	19.6	21.4	0.62	0.38	57.7	78.0	-	0.3	63.3
1308+182	0.21	0.62	-	21.0	29.4	0.79	0.71	64.3	113.3	-	0.6	110.1
1309−056	0.29	0.80	-	21.5	16.3	0.46	0.71	43.9	67.0	-	0.7	64.2
1309+340	0.32	0.60	-	22.7	5.4	0.05	0.40	15.4	20.5	-	0.9	22.7
1309+340	0.32	0.60	-	20.9	7.2	0.08	0.50	20.5	27.3	-	0.5	26.5
1318+29a	0.27	0.61	-	22.1	36.0	0.66	0.52	92.8	137.7	-	0.8	147.2
1331+170	0.19	0.76	0.744	21.0	27.6	0.64	0.84	56.1	112.2	0.7	0.6	102.5
1346−036	0.36	0.80	-	21.5	25.3	0.68	0.56	77.0	104.0	-	0.7	99.5
1416+067	0.14	0.53	-	22.0	8.2	0.15	0.56	13.3	29.8	-	0.7	33.2
1416+159	0.24	0.59	-	20.9	22.5	0.43	0.64	53.7	85.0	-	0.5	82.9
1421+122	0.22	0.71	-	21.3	13.6	0.30	0.76	30.6	54.3	-	0.6	52.2
1435+638	0.34	0.76	-	20.1	28.2	0.55	0.38	83.2	114.6	-	0.4	92.8
1517+239	0.22	0.76	0.738	21.2	35.1	0.81	0.78	79.3	143.0	1.1	0.6	133.8
1556+335	0.14	0.57	-	20.6	22.1	0.42	0.82	35.8	82.7	-	0.5	78.7
1559+173	0.34	0.69	-	22.2	4.4	0.03	0.51	13.1	17.6	-	0.8	18.3
1602−001	0.25	0.71	-	21.2	35.1	0.56	0.71	86.1	140.3	-	0.6	133.5
1634+176	0.25	0.68	-	20.8	2.2	0.01	0.68	5.4	8.6	-	0.5	8.0
2120+168	0.27	0.62	-	21.5	8.0	0.07	0.59	20.7	30.9	-	0.7	31.5
2145+067	0.22	0.80	0.790	19.7	47.9	0.97	0.60	108.1	197.1	3.1	0.3	143.8
2230+114	0.44	0.87	-	22.3	14.7	0.37	0.50	49.5	61.5	-	0.8	61.0

Notes to TABLE 6

Columns as in Table 5 except 12: the redshift z_l of the galaxy which would give it a luminosity of L_*, 13: the impact parameter corresponding to z_l.

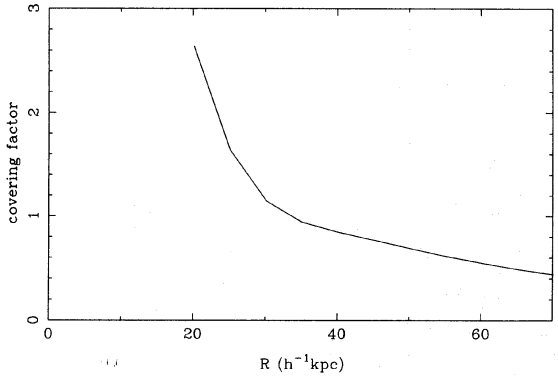

FIG. 4. Estimates of the covering factor for Mg II absorption derived from the distribution of galaxies close to the line of sight to all the quasars sampled. The model draws absorption systems from a uniform distribution of maximum radius R.

7. SUMMARY

In this paper we have presented a CCD imaging survey of bright quasars which we carefully searched for galaxies in the quasar fields. The important characteristics of our sample are its large size and the lack of any selection bias with respect to the presence of close galaxies. The quasars were selected independently of any knowledge of previously detected Mg II absorption. This enables us to make some important statistical conclusions about the absorption systems.

(1) As part of our statistical analysis we have defined and used a new statistic (S) to measure the significance of the distance to the closest galaxy to each quasar. This statistic is independent of the magnitude limit and galaxy surface density in each field. It is also insensitive to the effects of galaxy clustering which distort other measures such as the correlation function.

(2) We detect significantly large numbers of galaxies close to the lines of sight to quasars with Mg II absorption systems. These data are consistent with previous results implying that every Mg II absorption system is associated with a visible galaxy.

(3) The galaxies which are probably associated with the Mg II absorption systems are not significantly different from normal galaxies in either size or luminosity. We find no evidence for the large halos suggested by BB91, although we cannot rule them out at present. The distribution of impact parameters we measure is, however, flatter than detected by previous workers, suggesting that the absorption systems and galaxies may be part of extended structures $30h^{-1}$ kpc or greater in size.

(4) Our control sample of quasars without detected Mg II absorption also exhibits an excess of close galaxies. This may be due in part to a bias caused by gravitational lensing (see Paper II). Having a control sample enables us to estimate the covering factor in Mg II absorption for all the galaxies. We use a simple model of absorption systems with a constant covering factor out to a maximum radius of $30h^{-1}$ kpc from the observed galaxy. This model is consistent with a covering factor of unity. However, if we allow for incompleteness in our detection of the galaxies, the covering factor must then be smaller than unity.

(5) Finally, we have obtained similar results for a subsample of low redshift ($0.37 < z < 0.9$) quasars; a similar range of luminosities and impact parameters for four detected absorbers to that found for the high redshift sample. We do not find any evidence that this subsample is biased by the detection of galaxies in associated clusters at the

TABLE 7. Statistics of galaxies near quasars with low redshifts.

QSO (1)	z_1 (2)	z_2 (3)	z_{abs} (4)	m_{gal} (5)	r (6)	S (7)	p_z (8)	b_{z1} (9)	b_{z2} (10)	l_{mab} (11)	l_{abs} (12)	b_{abs} (13)
0710+118	0.47	0.76	-	21.4	21.2	0.71	0.33	73.4	86.2	-	-	0.0
0738+313	0.11	0.41	0.221	20.9	2.6	0.01	0.53	3.5	8.5	0.0	0.1	5.9
0738+313	0.11	0.41	0.221	21.5	9.5	0.15	0.44	12.6	30.9	0.0	0.1	21.5
0738+313	0.11	0.41	0.221	21.1	7.2	0.09	0.50	9.6	23.6	0.0	0.1	16.4
0742+318	0.11	0.48	0.192	20.5	14.4	0.44	0.74	19.1	50.2	0.0	0.1	29.4
0955+326	0.17	0.60	-	21.9	26.5	0.34	0.64	49.7	100.7	-	-	0.0
1049+616	0.11	0.41	0.225	19.1	2.9	0.01	0.79	3.9	9.4	0.0	0.6	6.6
1049+616	0.11	0.41	0.393	19.1	2.9	0.01	0.79	3.9	9.4	0.2	2.2	9.2
1103−006	0.14	0.53	-	19.6	15.0	0.30	0.82	24.3	54.7	-	-	0.0
1104+167	0.31	0.67	-	21.7	14.1	0.31	0.56	39.6	55.7	-	-	0.0
1318+29b	0.32	0.66	-	21.4	46.7	0.84	0.56	133.3	183.0	-	-	0.0
1354+195	0.22	0.80	0.456	21.7	7.0	0.07	0.80	15.8	28.8	0.2	0.3	23.9
1354+195	0.22	0.80	0.456	21.4	7.7	0.09	0.80	17.4	31.6	0.2	0.4	26.3
1512+370	0.28	0.39	-	19.9	10.5	0.14	0.27	27.6	33.3	-	-	0.0
1641+399	0.25	0.68	-	21.5	6.5	0.09	0.68	16.0	25.8	-	-	0.0
1704+608	0.11	0.41	0.163	20.4	6.7	0.05	0.62	8.9	21.7	0.1	0.1	12.2
1704+608	0.11	0.41	0.222	20.4	6.7	0.05	0.62	8.9	21.7	0.1	0.2	15.1
1828+487	0.25	0.71	-	20.1	9.2	0.11	0.60	22.7	37.0	-	-	0.0

Notes to TABLE 7
Columns as for Table 5.

quasar redshift, but these low redshift quasars are treated separately because of this possibility.

We thank D. Millar and M. Neeser for assistance with the observations. M. Colless provided software for the calculation of galaxy colors and k corrections. Mont Mégantic Observatory is supported by grants from NSERC (Canadian Government) and FCAR (Québec Government). R.L.W. acknowledges support from NSERC, and M.J.D. thanks MESS (Québec Government) for travel funds. The staff of Central Computing Services, NOAO have given invaluable help with their support of the IRAF software. We are grateful to A. Hewitt and G. Burbidge for providing copies of Hewitt & Burbidge (1989). This research has made use of the NASA/IPAC Extragalactic Database which is operated by the Jet Propulsion Laboratory, California Institute of Technology, under contract with the National Aeronautics and Space Administration.

APPENDIX

We provide a summary here of the expressions used to calculate the various quantities given in the tables above.

1. Impact Parameter

In a standard Friedman cosmology, the proper distance is given by

$$d=\frac{cf(z,\Omega_0)}{H_0(1+z)}, \tag{1}$$

with

$$f(z,\Omega_0)=\begin{cases} z\left(1+\frac{z}{2}\right), & \Omega_0=0, \\ \dfrac{\Omega_0 z-(2-\Omega_0)(\sqrt{1+\Omega_0 z}-1)}{\frac{1}{2}\Omega_0^2}, & \Omega_0>0, \end{cases} \tag{2}$$

(see Weedman 1986). The impact parameter, measured in comoving units, between the line of sight to a quasar and a galaxy at redshift z, θ radians from the line of sight is then given by

$$b(\mathrm{Mpc})=\frac{\theta c}{H_0}\frac{1}{(1+z)^2}f(z,\Omega_0), \tag{3}$$

where the Hubble constant is given as $H_0=100h$ km s^{-1} Mpc^{-1}. We adopt a value of $\Omega_0=1$ throughout.

2. Luminosity

To define an absolute magnitude in the rest frame for our galaxies we have taken the values of Binney & Tremaine (1987) with $L_*=1.0\times10^{10}h^{-2}L_\odot$, and $M_{V\odot}=+4.83$, so

$$M_{*V}=-20.17+5\log_{10}h, \tag{4}$$

$$M_{*R}=-20.17+5\log_{10}h+(R-V), \tag{5}$$

where $(R-V)\approx-0.72,-0.62,-0.54,-0.44,-0.40$ for galaxy types E/S0, Sa/Sb, Sb/Sc, Sc/Sd, and Sdm/Irr, respectively. The relation between absolute magnitude, M, apparent magnitude, m, and redshift is

$$M=m-5\log_{10}\left(\frac{cf}{H_0}\frac{1}{10^{-5}\ \mathrm{Mpc}}\right)-k(z,\mathrm{type}), \tag{6}$$

where $k(z,\mathrm{type})$ is the k correction which takes into account the differing amount of flux falling into the observed band due to redshifting of the galaxy spectrum. In general the k correction is largest for early-type galaxies as they fall off more rapidly to the blue. Here we used values for the Sbc galaxy type (consistent with disks). At a redshift of 0.7 this would introduce maximum errors of -0.65 mag for E/S0s to $+0.45$ mag for Sdm/Irr galaxies. The galaxy colors and k-corrections used here were calculated from standard spectral energy distributions with software kindly supplied by M. Colless.

We can now use Eqs. (5) and (6) to write an expression for the luminosity of the galaxy in terms of L_*:

$$L/L_*=10^{0.4(M_*-M)}$$
$$=10^{0.4[-20.17+(r-v)-m+k(z,\mathrm{type})]}\left(\frac{cf}{10^{-3}\ \mathrm{km\ s^{-1}}}\right)^2. \tag{7}$$

Note that the terms in h cancel, making this measure of the galaxy luminosity independent of the Hubble constant.

3. Measured Spectral Region

Our aim here is to determine the probability that a galaxy with apparent magnitude m_g has a redshift in the range $[z_1,z_2]$, given that it is drawn from the standard luminosity function. To do this we tabulate integral counts of galaxies as a function of redshift. We define $nz(m_g,\delta m,z')d\Omega$ as the number of galaxies observed with magnitudes in the range m_g, $m_g+\delta m$ and redshifts $0<z<z'$ in a solid angle $d\Omega$, given by

$$nz(m_g,\delta m,z')d\Omega=\int_0^{z'}dz\frac{dV}{dz}\Phi[L(m,z)]dL(m_g,\delta m,z), \tag{8}$$

where the volume element is

$$\frac{dV}{dz}=\left(\frac{c}{H_0}\right)^3\frac{[f(z,\Omega_0)]^2}{(1+z)^3\sqrt{1+\Omega_0 z}}d\Omega, \tag{9}$$

and the luminosity interval corresponding to δm is approximated by

$$dL\approx L(m_g,z)-L(m_g+\delta m,z). \tag{10}$$

The luminosity function has a standard Schechter form with a constant comoving number density and no luminosity evolution, written as

$$\Phi(L)dL=\frac{\mathscr{L}}{L_*\Gamma(2+\alpha)}\left(\frac{L}{L_*}\right)^\alpha\exp\left(-\frac{L}{L_*}\right)\frac{dL}{L_*}, \tag{11}$$

with $\alpha = -1.25$ and the luminosity density normalization $\mathscr{L} = (1.7 \pm 0.6) \times 10^8 h L_{\odot V}$ Mpc^{-3} (Binney & Tremaine 1987).

The probability of detection is then given by

$$p_z(m_g, z1, z2) = \frac{nz(m_g, \delta m, z_2) - nz(m_g, \delta m, z_1)}{nz(m_g, \delta m, 1.0)}, \quad (12)$$

where we normalize to the number of galaxies detected with $z < 1.0$ since, at the magnitude limits discussed here no significant numbers of galaxies are detected at higher redshifts.

4. Most Probable Redshift

The columns in the tables labeled z_l give the redshift at which a galaxy would have luminosity L_*. This was calculated by numerically solving Eq. (7) for the value of z at which $L/L_* = 1$.

REFERENCES

Arnaud, J., Hammer, F., Jones, J., & Le Fèvre, O. 1988, A&A, 206, L5
Bahcall, J. N., & Spitzer, L. 1969, ApJ, 156, L63
Bechtold, J., & Ellingson, E. 1992, ApJ, 396, 20
Bergeron, J. 1988, in IAU Symposium No. 130, edited by J. Audouze, M.-C. Pelletan, and A. Szalay (Kluwer, Dordrecht), p. 343
Bergeron, J., & Boissé, P. 1991, A&A, 243, 344 (BB91)
Binney, J., & Tremaine, S. 1987, Galactic Dynamics (Princeton University Press, Princeton)
Boulade, O., Kunth, D., Tytler, D., & Vigroux L. 1987, in High Redshift and Primeval Galaxies, edited by J. Bergeron *et al.* (Editions Frontières, France), p. 349
Bregman, J. N., *et al.* 1986, ApJ, 301, 708
Christian, C. A., Adams, M., Barnes, J. V., Butcher, H., Hayes, D. S., Mould, J. R., & Siegel, M. 1985, PASP, 97, 363
Christian, C. A., Crabtree, D., & Waddell, P. 1987, ApJ, 312, 45
Cristiani, S. 1987, ApJ, 175, L1
Drinkwater, M., & Hardy, E. 1991, AJ, 101, 94
Drinkwater, M. J. 1993, The Observatory, 113, 40
Ellingson, E., Green, R. F., & Yee, H. K. C. 1991, ApJ, 378, 476
Foltz, C. B., Weyman, R. J., Peterson, B. M., Sun, L., Malkan, M. A., & Chaffee, F. H. 1986, ApJ, 307, 504
Harris, W. E. 1990, PASP, 102, 949
Harris, W. E., Allwright, J. W. B., Pritchet, C. J., & van den Berg, S. 1991, ApJS, 76, 115
Hewitt, A., & Burbidge, G. 1987, ApJS, 63, 1
Hewitt, A., & Burbidge, G. 1989, ApJS, 69, 1
Hickson, P., & Hutchings, J. B. 1987, ApJ, 312, 518
Hutchings, J. B. 1990, PASP, 102, 431
Hutchings, J. B., & Neff, S. G. 1990, AJ, 99, 1715
Kent, S. 1985, PASP, 97, 165
Lanzetta, K., & Bowen, D. 1990, ApJ, 357, 321
Maddox, S. J., Sutherland, W. J., Efstathiou, G., & Loveday, J. 1990, MNRAS, 243, 692
Miller, J. S., Goodrich, R. W., & Stephens, S. A. 1987 AJ, 94, 633
Nottale, L. 1988, Ann. Phys. Fr., 13, 223
Petitjean, P., & Bergeron, J. 1990, A&A, 231, 309
Pritchet, C., & Kline, M. I. 1981, AJ, 86, 1859
Roy, J.-R. 1990, private communication
Sargent, W. L. W., Steidel, C. C., & Boksenberg, A. 1988, AJ, 334, 22
Savage, B. D., *et al.* 1993, preprint
Steidel, C. C., & Sargent, W. L. W. 1992, ApJS, 80, 1
Thomas, P. A., & Webster, R. L. 1990, ApJ, 349, 437
Tytler, D., Boksenberg, A., Sargent, W. L. W., Young, P. J., & Kunth, D. 1987, ApJS, 64, 667
Valdes, F. 1982a, FOCAS User's Manual, Kitt Peak National Observatory, Tucson
Valdes, F. 1982b, in Instrumentation in Astronomy IV, Proc. SPIE, 331, 465
Vidal-Madjar, A., Andreani, P., Cristiani, S., Ferlet, R., Lanz, T., Vladilo, G. 1987, A&A, 177, L17
Weedman, D. 1986, Quasar Astronomy (Cambridge University Press, Cambridge)
Weyman, R. J., Williams, R. E., Peterson, B. M., & Turnsheck, D. A. 1979, ApJ, 234, 33
Yee, H. K. C., Green R. F., & Stockman, H. S. 1986, ApJS, 62, 681 (YGS)
York, D. G. 1988, in QSO Absorption Lines: Probing the Universe, edited by J. C. Blades, D. Turnsheck, and C. A. Norman (Cambridge University Press, Cambridge), p. 227
Young, P., Gunn, J. E., Kristian, J., Oke, J. B., & Westphal, J. A. 1980, ApJ, 241, 507
Young, P., Sargent, W. L. W., & Boksenberg, A. 1982, ApJS, 48, 455